



Medical Image Analysis on Left Atrial LGE MRI for Atrial Fibrillation Studies: A Review

Lei Li^{a,b,c}, Veronika A. Zimmer^{c,d}, Julia A. Schnabel^{c,d,e}, Xiahai Zhuang^{*a}

^aSchool of Data Science, Fudan University, Shanghai, China

^bSchool of Biomedical Engineering, Shanghai Jiao Tong University, Shanghai, China

^cSchool of Biomedical Engineering and Imaging Sciences, King's College London, London, UK

^dDepartment of Informatics, Technical University of Munich, Germany

^eHelmholtz Center Munich, Germany

ARTICLE INFO

Article history:

Received 16 June 2021

Keywords: Atrial fibrillation, LGE MRI, Left atrium, Review

ABSTRACT

Late gadolinium enhancement magnetic resonance imaging (LGE MRI) is commonly used to visualize and quantify left atrial (LA) scars. The position and extent of scars provide important information of the pathophysiology and progression of atrial fibrillation (AF). Hence, LA scar segmentation and quantification from LGE MRI can be useful in computer-assisted diagnosis and treatment stratification of AF patients. Since manual delineation can be time-consuming and subject to intra- and inter-expert variability, automating this computing is highly desired, which nevertheless is still challenging and under-researched.

This paper aims to provide a systematic review on computing methods for LA cavity, wall, scar and ablation gap segmentation and quantification from LGE MRI, and the related literature for AF studies. Specifically, we first summarize AF-related imaging techniques, particularly LGE MRI. Then, we review the methodologies of the four computing tasks in detail, and summarize the validation strategies applied in each task. Finally, the possible future developments are outlined, with a brief survey on the potential clinical applications of the aforementioned methods. The review shows that the research into this topic is still in early stages. Although several methods have been proposed, especially for LA segmentation, there is still large scope for further algorithmic developments due to performance issues related to the high variability of enhancement appearance and differences in image acquisition.

© 2021 Elsevier B. V. All rights reserved.

1. Introduction

1.1. Clinical goals

Atrial fibrillation (AF) is the most common cardiac arrhythmia encountered in the clinic, occurring in up to 2% of the population and rising in prevalence along with advancing age (Chugh et al., 2014). Fig. 1 presents the comparison of sinus rhythm and AF. One can see that there are chaotic elec-

trical signals in the atrium of AF patients compared to sinus rhythm, resulting in a rapid and irregular heart rhythm. Radiofrequency catheter ablation via pulmonary vein isolation (PVI) is a promising procedure for treating AF, especially for paroxysmal AF patients (Calkins et al., 2007). The left atrium (LA) is a crucial structure in the pathophysiology of AF, and the observation of LA remodeling can be important for initial evaluation of AF (Tops et al., 2010). Besides, structural changes in the LA wall (especially changes in the wall thickness) are known to occur in AF patients (Karim et al., 2018). The wall thickness can be used to predict the response to invasive treat-

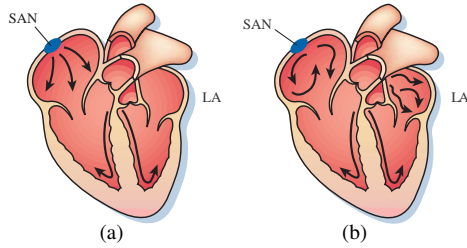


Fig. 1. The electrical activity in left atrium (LA): (a) sinus rhythm; (b) atrial fibrillation (AF). The sinoatrial node (SAN) produces an electrical impulse, which is regular in the sinus rhythm and can be overwhelmed by disorganized electrical waves, usually originating from the pulmonary veins. Here, the images are modified from Nattel (2002).

Table 1. AF patient classification depending on fibrosis extent (Akoum et al., 2011).

Utah grade	Percentage	Success rate	AF recurrence
Utah 1 (minimal)	$\leq 5\%$	100%	0
Utah 2 (mild)	5~20%	81.8%	28%
Utah 3 (moderate)	20~35%	62.5%	35%
Utah 4 (extensive)	$\geq 35\%$	0	56%

ment of AF and has the potential for improving the safety of AF ablation (Whitaker et al., 2016). The wall thickness is also important to measure the transmuralty of scars which is related to the AF recurrence (Ranjan et al., 2011). The success of AF treatments is highly related to the formation of contiguous scar completely encircling the veins (Ranjan et al., 2011). Unfortunately, the encircling lesion is often incomplete with a combination of ablation scars and gaps of healthy tissue (Miller et al., 2012). Therefore, the extent and distribution of both scars and gaps are important information for AF patient selection (Akoum et al., 2011), diagnosis prediction (Arujuna et al., 2012), and treatment stratification (Njoku et al., 2018). For example, patients were divided into four grades according to their degrees of fibrosis (refers to preexisting scars) in Akoum et al. (2011), shown in Table 1. Based on the scoring, various therapeutic strategies were suggested by electrophysiologists.

Recently, late gadolinium enhancement magnetic resonance imaging (LGE MRI) has evolved as a tool for defining the extent of fibrosis/ scars and visualizing the ablation gaps (Siebermair et al., 2017; Li et al., 2020b; Nuñez-Garcia et al., 2019). Therefore, it is crucial to develop techniques for the four progressive tasks, i.e., (1) LA segmentation, (2) LA wall segmentation together with wall thickness measurement, (3) scar segmentation and quantification, and (4) ablation gap localization from LGE MRI. Fig. 2 provides the clinical pipeline for AF ablation procedures, where the role of LGE MRI is highlighted and the four closely related tasks of clinical interests are presented, followed by several related clinical applications.

1.2. Challenges and public datasets

Manual delineations of the LA, LA wall, scars and ablation gaps are all labor-intensive and prone to be subjective, so their automation is highly desired, which nevertheless remains challenging. The challenges for automatic LA segmentation are mainly from the large variations in terms of LA shape, inten-

sity range as well as poor image quality. For the LA wall analysis, two additional difficulties are presented, i.e., the intrinsic thin wall thickness and the complex structure of the LA wall. Here, the complex structure refers to the multiple openings in its 3D structure such as the pulmonary veins (PV) and mitral valve (MV) of the LA. For the scar analysis, its unique challenge lies in the enhanced noise from surrounding tissues. For the gap quantification, the large variability in PV morphology (position, orientation, size, thickness) and the robustness to scar segmentation changes are the two major concerns. Fig. 3 illustrates and explains part of these challenges in an intuitive way.

Due to the challenges of these tasks, several challenge events are organized in recent years at the international conferences such as ISBI (International Symposium on Biomedical Imaging) and MICCAI (Medical Image Computing and Computer-Assisted Interventions), with corresponding public dataset releases. For example, Karim et al. organized the *Left Atrium Fibrosis and Scar Segmentation Challenge* at ISBI 2012. They provided 60 multi-center and multi-vendor LGE MRIs with the manual labels of both LA and scars, and summarized the submitted algorithms from seven institutions in Karim et al. (2013). Tobon-Gomez et al. organized the *Left Atrium Segmentation Challenge*, in conjunction with STACOM'13 workshop and MICCAI'13. They offered a dataset including 30 CT and 30 MRIs with the manual LA segmentation, and presented the results of nine algorithms for CT and eight algorithms for MRI in Tobon-Gomez et al. (2015). Their results showed that the methodologies that combined statistical models with region-growing methods were the most suitable for the proposed task. In 2016, Karim et al. organized another challenge event, i.e., *Left Atrial Wall Thickness Challenge*, in conjunction with STACOM'16 workshop and MICCAI'16. The released images consisted of 10 CT and 10 MRI of healthy and diseased subjects. Only two of the three participants contributed to the automatic segmentation of the computed tomography (CT) data, but no work on the MRI data was reported (Karim et al., 2018). The limited number of submitted algorithms generally performed poorly compared to the inter-observer variability, which reveals the difficulty of the wall segmentation task. In 2017, Zhuang et al. organized the *Multi-Modality Whole Heart Segmentation Challenge*, in conjunction with STACOM'17 workshop and MICCAI'17. They provided 120 multi-modality images covering a wide range of cardiac diseases, such as AF, myocardial infarction and congenital heart disease (Zhuang et al., 2019). Ten algorithms for CT data and eleven methods for MRI data have been evaluated, and most of the submitted algorithms were based on deep learning (DL). The evaluated results showed that the LA segmentation of AF patients was particularly more accurate compared to other categories of patients. Zhao et al. organized the *Atrial Segmentation Challenge*, in conjunction with STACOM'18 workshop and MICCAI'18. They provided 150 LGE MRIs with manual LA segmentations generated from three experts, and the data covers both pre- and post-ablation images (Xiong et al., 2020). To explore the quality of the dataset, they calculated three measures, i.e., signal to noise ratio (SNR), contrast ratio (CR), and heterogeneity (HET), which were in agreement. The quality measurements showed that

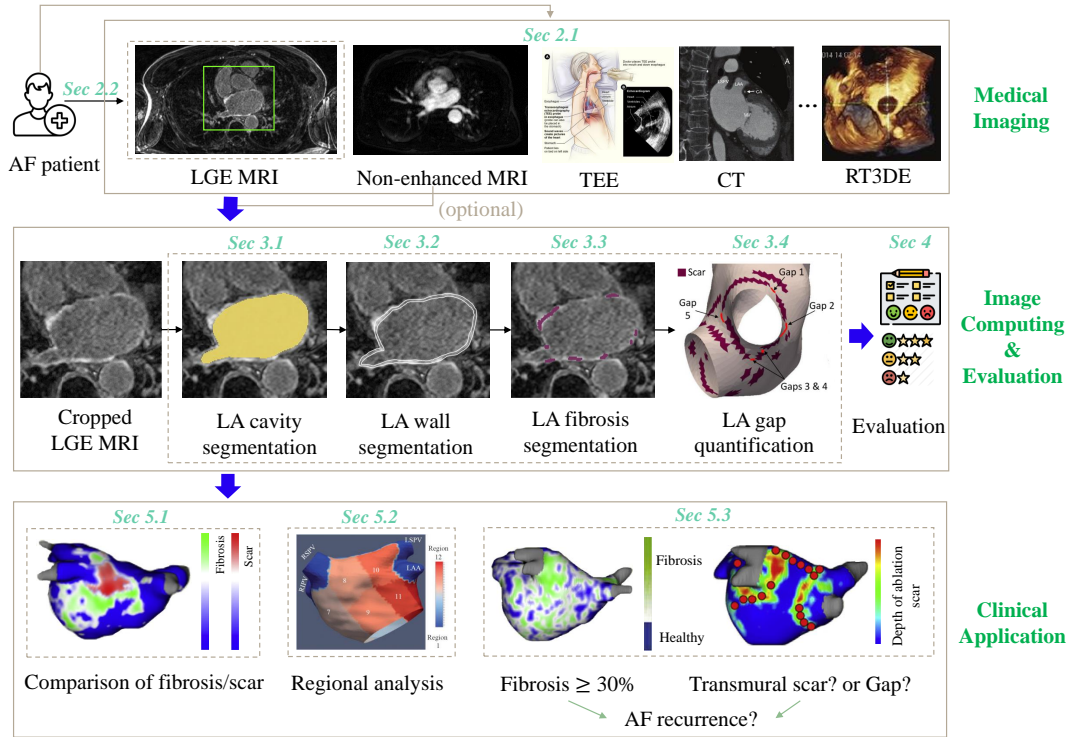


Fig. 2. The pipeline of LA image computing for AF studies and the structure of this review. Top row: common image modalities for AF treatments: LGE MRI, non-enhanced MRI, transesophageal echocardiography (TEE) (image adapted from *Stanford HEALTH CARE*), CT, and real-time 3D echocardiography (RT3DE) (image adapted from Regazzoli et al. (2015)); Middle row: computation and evaluation steps for LA analysis reviewed in this study (images adapted from Li et al. (2020c); Nuñez-Garcia et al. (2019)); Bottom row: possible clinical applications (images adapted from Siebermair et al. (2017); Benito et al. (2018)).

Table 2. Summary of the public datasets whose research targets are AF patients or include AF patients. Here, the star (*) indicates that the data is acquired from multiple centers and vendors.

Source	Year	Data	Target	Name & Link
Utah (2012)	2012	155 LGE MRI + 3D MRI	LA, LA wall	CARMA, University of Utah
Karim et al. (2013)	2012	60 LGE MRI*	LA scar	Left Atrium Fibrosis and Scar Segmentation Challenge
Tobon-Gomez et al. (2015)	2013	30 CT, 30 bSSFP MRI	LA	Left Atrium Segmentation Challenge
Karim et al. (2018)	2016	10 CT, 10 black-blood MRI	LA wall	Left Atrial Wall Thickness Challenge
Zhuang et al. (2019)	2017	60 CT, 60 bSSFP MRI*	Whole heart	Multi-Modality Whole Heart Segmentation Challenge
Xiong et al. (2020)	2018	150 LGE MRI	LA	Atrial Segmentation Challenge

less than 15% of the data had high quality ($\text{SNR} > 3$), 70% had medium quality ($\text{SNR} = 1 \sim 3$), and over 15% was of low quality ($\text{SNR} < 1$). In total, 27 teams contributed to the automatic LA segmentation, and most of the methods were DL-based except for two multi-atlas segmentation (MAS) methods. The results proved that two-stage convolutional neural networks (CNNs) achieved superior results than other single CNN methods and conventional methods (non DL-based methods). This challenge event provided a significant step towards much-improved segmentation methods on LA segmentation of LGE MRI.

In summary, these challenge events promoted dedicated research on these tasks, and offer open and fair competitions for various research groups to test and validate their algorithms. Table 2 summarizes the public AF related events and datasets with corresponding download links.

1.3. Study inclusion and literature search

In this work, we aim to provide the reader with a survey of the state-of-the-art image computing techniques, important results as well as the related literature for AF studies. To ensure comprehensive coverage, we have screened publications during the last 10 years related to this topic. Our main sources of references were Internet searches using engines such as Google scholar, PubMed, IEEE-Xplore, and Citeseer. To cover as many related works as possible, flexible search terms have been employed when using these search engines, as summarized in Table 3. Both peer-reviewed journal papers and conference papers were included here. We have also followed the references found in papers from these sites, and finally collected a comprehensive library of more than 130 papers. Fig. 4 presents the distributions of papers in segmentation and quantification from LGE MRI for AF patients per year/task. Note that we generally picked the most detailed and representative ones for this

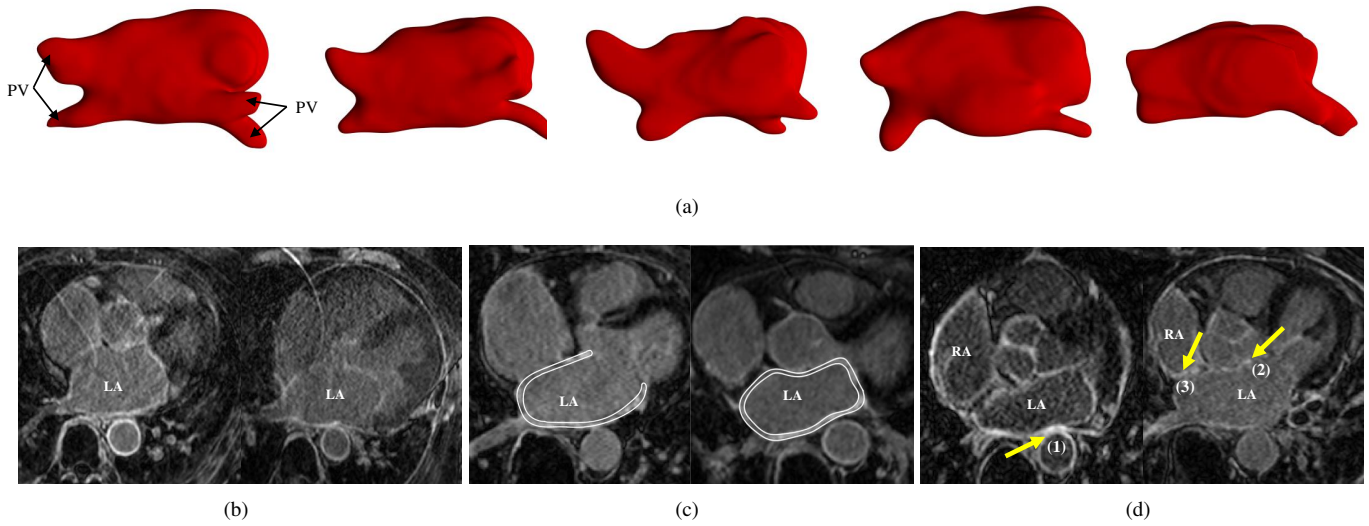


Fig. 3. The challenges of automatic segmentation and quantification of LGE MRI for AF: (a) various LA and pulmonary vein (PV) shapes; (b) two typical LGE MRIs with poor quality; (c) thin atrial walls highlighted using bright white color in the figure; (d) surrounding enhanced regions pointed out by the arrows, where (1) and (2) indicate the enhanced walls of descending and ascending aorta, respectively; and (3) denotes the enhanced walls of right atrium (RA). Images (b)-(d) adopted from Li *et al.* (2020b).

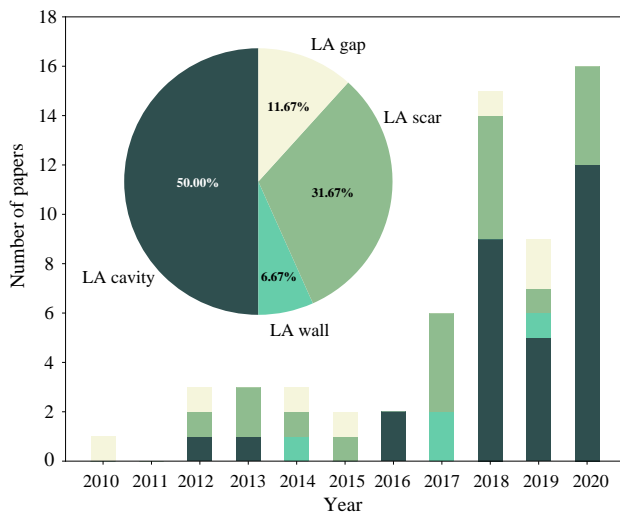


Fig. 4. The distributions of papers of LGE MRI segmentation and quantification for AF patients per year and task.

review when we encountered several papers from the same authors about the same subject.

1.4. Related review literature

Table 4 lists existing review papers related to AF. One can see that most current AF related review papers focused on a clinical survey instead of the methodology of image computing, such as segmentation or quantification algorithms. Only two reviews, Pontecorboli *et al.* (2017) and Jamart *et al.* (2020), are similar to ours in terms of topic (LGE MRI) and style (technical). However, only conventional thresholding methods or only DL-based methods were reviewed in each work. Fig. 5 visualizes the scopes of current reviews as well as this review, and one can see that the scopes are different though with partial overlaps. Besides, our review organizes the related works

Table 3. Search engines and expressions used to identify potential papers for review.

Engine	Google scholar, PubMed, IEEE-Xplore, and Citeseer
Term	<p>“Atrial fibrillation” or AF and</p> <p>“Late gadolinium/ delayed enhancement/ contrast enhanced (cardiac) magnetic resonance” or “LGE/ DE/ CE MR(I)” or “LGE-/ DE-/ CE-MR(I)” or “LGE/ DE/ CE CMR” or “LGE-/ DE-/ CE-CMR” and</p> <p>Classif*/ segment*/ quantif*/ localiz*/ detect* and</p> <p>“Left atrium/ atrial” or LA or</p> <p>“Atrial wall/ myocardi*” or “wall thickness” or</p> <p>“Atrial scars/ fibrosis/ lesion” or “ablation pattern” or</p> <p>“Ablat*”/ lesion gaps” or “gaps in ablation lesion” or “in-complete ablation pattern”</p>

according to the clinical pipeline (see Fig. 2), resulting in an intuitive structure of the paper.

1.5. Structure of this review

The remainder of the paper is organized as follows (compare Fig. 2): Section 2 presents the current common imaging tools used in AF ablation and the importance of LGE MRI in the management of AF. Section 3 systematically reviews the state-of-the-art image computing techniques and results of LA cavity, wall, scar and ablation gap segmentation and quantification. Section 4 presents the data and evaluation measures for each task. Potential clinical applications are provided in Section 5. Discussion of current LA LGE MRI computing challenges and the future perspectives are given in Section 6, along with a conclusion in Section 7.

2. Imaging of AF

Medical images can offer crucial information for the evaluation and treatment of AF patients, and have been widely used

Table 4. Summary of the review papers related to AF. EAM: electroanatomical mapping; JAF: Journal of Atrial Fibrillation; JACC: Journal of the American College of Cardiology; RMPBM: Magnetic Resonance Materials in Physics, Biology and Medicine; JICRM: The Journal of Innovations in Cardiac Rhythm Management; FCM: Frontiers in Cardiovascular Medicine; CET: Cardiovascular Engineering and Technology.

Source	Venue	Scope	Limitation
Cox (2003)	Europace	Surgical treatment of AF	Clinical review
Rolf et al. (2014)	JAF	EAM of AF	Clinical review
Dzeshka et al. (2015)	JACC	Mechanisms and clinical implications of AF	Clinical review
Whitaker et al. (2016)	Europace	Wall thickness measurement for CT	Target image is not LGE MRI
Peng et al. (2016)	RMPBM	Cardiac chamber segmentation	Target partially includes LA cavity
Pontecoroli et al. (2017)	Europace	Fibrosis segmentation from LGE MRI	Only thresholding methods are included
Siebermair et al. (2017)	JACC	LGE fibrosis imaging	Clinical review
Obeng-Gyimah and Nazarian (2020)	JICRM	Imaging for AF ablation	Clinical review
Jamart et al. (2020)	FCM	LA segmentation from LGE MRI	Only DL-based methods are included
Chen et al. (2020)	FCM	DL-based cardiac segmentation	Target partially includes LA and its scars
Habijan et al. (2020)	CET	Whole heart and chamber segmentation	Target partially includes LA cavity

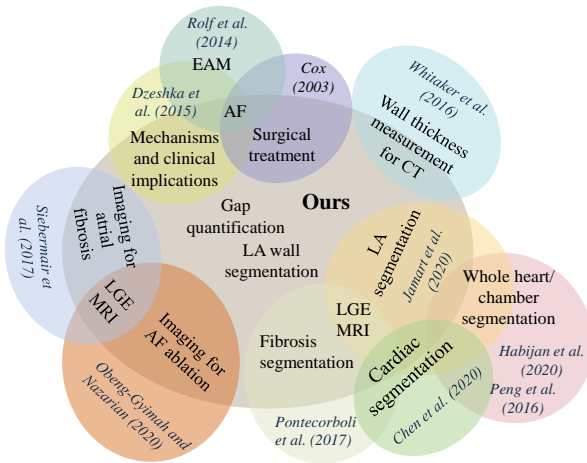


Fig. 5. Comparison in the scope with related review studies via Venn diagram.

in the ablation process (Tops et al., 2010; Obeng-Gyimah and Nazarian, 2020). Table 5 summarizes the common imaging modalities used in three ablation stages. One can see that diverse imaging modalities have been introduced in the ablation process, each of which assists in various aspects of the procedure.

2.1. Imaging during ablation procedure

Before catheter ablation (CA), the first step is to exclude contraindication, such as the LA appendage (LAA) thrombi which are normally detected using transesophageal echocardiography (TEE) (Calkins et al., 2007). MRI and CT can be used to detect LA thrombi, but both of them tend to have low inter-observer agreement (Mohrs et al., 2006; Gottlieb et al., 2008). To select patients expected for successful CA, the assessment of LA, PVs and fibrosis are the key steps (Berruezo et al., 2007; Akoum et al., 2011). Three-dimensional (3D) imaging techniques such as CT or MRI are generally used for PV anatomy assessment. PV anatomy can also be measured well by TEE, achieving up to 95% concordance with MRI (Toffanin et al., 2006). Moreover, cardiac MRI remains the gold standard for fibrosis assessment (Obeng-Gyimah and Nazarian, 2020). Especially, LGE MRI

appears to be a promising alternative for pre-ablation scar visualization and quantification (Siebermair et al., 2017).

During CA, fluoroscopy is the most commonly employed imaging technique in the electrophysiology laboratory. Intracardiac echocardiography (ICE) offers real-time imaging of the PVs and adjacent structures, and enhances the safety of transseptal puncture by visualizing inter-atrial septum and puncture needle (Jongbloed et al., 2005). Both ICE and fluoroscopy can visualize the LA and PVs (Saad et al., 2002). Note that the integration of different imaging modalities during CA is promising (Tops et al., 2010), but is out of the scope of this review.

After CA and during the follow-up study, the main target of post-procedural imaging is to monitor complications and help predict recurrence. The most frequently occurring complications of AF ablation include PV stenosis, pericardial effusion and atrio-oesophageal fistula. Multi-slice CT and MRI are usually used for the accurate assessment of PV stenosis and esophageal injury (Holmes et al., 2009). Transthoracic echocardiography (TTE) is a recommended imaging tool for screening to detect pericardial effusion (Calkins et al., 2007). To predict recurrence, LA size and functions are important indices, as LA ablation can lead to the formation of scars and subsequent changes in LA anatomy (Casaclang-Verzosa et al., 2008). *For the follow-up analysis of LA volumes*, TTE is typically used, but 3D techniques, such as real-time 3D echocardiography (Zhang et al., 2017), multi-slice CT (Polaczek et al., 2019) and MRI (Tsao et al., 2005), especially LGE MRI (McGann et al., 2014), may provide more accurate information. *For the measurement of LA wall thickness*, TEE provides high spatial resolution and has been used by Bakalli et al. (2012). CT is an ideal modality, thanks to its high resolution, and MRI is widely considered to be the gold standard for the viability assessment of wall pathology (Karim et al., 2018).

LGE MRI has been recently widely explored for scar and ablation gap quantification (Nuñez-García et al., 2019; Mishima et al., 2019). Note that T1-weighted MRI has become an imaging marker for diffused cardiac fibrosis, and has been validated against histological studies (Sibley et al., 2012). Nevertheless, it can be difficult to localize fibrosis using T1 MRI, and it is therefore not appropriate for ablation procedure guidance

Table 5. The role of different imaging modalities in the AF ablation procedure. CA: catheter ablation; LAA: LA appendage; ICE: intracardiac echocardiography; TTE: transthoracic echocardiography.

Stage	Target	Imaging modality	Important summary
Before CA	Assessment of LAA thrombus	TEE CT/ MRI	Gold standard for LAA thrombi identification Low inter-observer agreement
	Assessment of LA size and anatomy	TEE RT3DE CT/ (LGE) MRI	The most commonly used imaging technique in daily clinical practice New technique for the assessment of LA volumes Gold standard for the assessment of LA volumes
	Assessment of PV anatomy	TEE/ CT/ MRI	Provides detailed 3D information on PV anatomy as a “road-map” for ablation
	Assessment of fibrosis	(LGE) MRI	Gold standard for evaluating fibrosis; predicts AF recurrence following ablation
During CA	Positioning catheters	Fluoroscopy	Standard imaging modality in the electrophysiology laboratory; used to visualize catheters and devices
	Transseptal puncture	ICE	Used to enhance the safety of transseptal puncture and catheter tissue contact; used to visualize inter-atrial septum and puncture needle
	Visualization of LA and PVs	Fluoroscopy ICE	New rotational angiography technique to accurately identify PV anatomy and diameters Real-time assessment of PV ostium with a limitation on the detection of small proximal branches from PVs
After CA	Assessment of PV stenosis	CT/ MRI	Preferably, these 3D techniques are correlated with pre-procedural images for detection of PV stenosis
	Detection of pericardial	TTE	Routine echocardiography should be performed before discharge and during the follow-up study
	Esophageal injury	CT/ MRI TTE	Performed when atrio-oesophageal fistula is suspected Conventional method for the detection of LA volumes and function
	Assessment of LA size and function	RT3DE/ CT/ (LGE) MRI	3D assessment of LA volumes allows the detection of LA reverse remodelling
	Assessment of wall thickness	TEE/ CT/ (LGE) MRI	Increased atrial wall thickening was seen in the post-ablation scans
	Assessment of scars and gaps	LGE MRI T1-weighted MRI	Promising in the ablation lesion visualization New technique without contrast agent for the assessment of scars

or ablation gap identification. LGE MRI remains a promising method to detect focal and cohesive fibrosis (Pontecorboli *et al.*, 2017).

2.2. LGE MRI for AF studies

LGE MRI is mainly used to evaluate fibrosis and scars of AF patients before and after ablation. This is because LGE MRI can discriminate scarring and healthy tissues by their altered wash-in and wash-out contrast agent kinetics (Marrouche *et al.*, 2014). Scars are thus visualized as the regions of being enhanced or high signal intensity compared to healthy tissues (Yang *et al.*, 2018a). There is still no consensus on the option and dosage of the contrast agent, nor on the timing of image acquisition after contrast administration, as Table 6 shows. Among the listed protocols, the DECAAF (Delayed-Enhancement MRI Determinant of Successful Radiofrequency Catheter Ablation of Atrial Fibrillation) protocol can be considered the most widely used one for LA fibrosis imaging (Siebermair *et al.*, 2017). Considering the importance and advances of LGE MRI in AF studies, in this review we mainly focus on the computing works on LGE MRI.

3. Image computing

We structure the review of image computing methodology according to the segmentation and quantification of the anatomical structures in question, as presented in Fig. 2.

3.1. LA cavity segmentation

In recent years, many algorithms have been proposed to perform automatic LA segmentation from medical images, but mostly for non-enhanced imaging modalities. Conversely, limited number of works of the LA segmentation from LGE MRI were reported in the literature before 2018. Most of the current studies on LA segmentation from LGE MRI are still based on time-consuming and error-prone manual segmentation methods (Higuchi *et al.*, 2018; Njoku *et al.*, 2018). This is mainly because LA segmentation methods in non-enhanced imaging modalities are difficult to directly apply to LGE MRI, due to the existence of contrast agents and low-contrasted boundaries in LGE MRI. Therefore, existing conventional automatic LA LGE MRI segmentation approaches generally require additional information, such as shape priors (Zhu *et al.*, 2013) or other MRI sequences (Ravanelli *et al.*, 2014; Tao *et al.*, 2016a; Li *et al.*, 2020b). Recently, with the development of DL in medical image processing, numerous DL-based algorithms are proposed

Table 6. Imaging parameters for LGE scar assessment utilized in several leading centers worldwide. SA: Siemens Avanto; PA: Philips Achieva; TR: repetition time; TE: echo time; Acq. T: acquired time after contrast agent injection; CARMA: Comprehensive Arrhythmia Research and Management; DECAAF: Delayed-Enhancement MRI Determinant of Successful Radiofrequency Catheter Ablation of Atrial Fibrillation. Here, [†] refers to multiply centers.

Source	Center	Scanner	TR/TE (ms)	Acq. T (min)	Gadolinium dose	Spacing (mm ³)
Badger et al. (2010)	Utah, USA	1.5 T, SA	5.5/2.3	15	0.1 mmol/kg	1.25 × 1.25 × 2.5
Taclar et al. (2010)	Boston, USA	1.5 T, PA	3.8/1.52	15~25	0.2 mmol/kg	1.3 × 1.3 × 4.0/5.0
Hunter et al. (2013)	Imperial/Barts, UK	1.5 T, PA	N/A	20	0.4 mmol/kg	1.5 × 1.5 × 4.0
Bisbal et al. (2014)	Barcelona, Spain	3 T	2.3/1.4	25~30	0.2 mmol/kg	1.25 × 1.25 × 2.5
McGann et al. (2014)	CARMA [†]	1.5 T; 3 T, SA	5.2/2.4; 3.1/1.4	5~9; 6~12	0.1 mmol/kg	1.25 × 1.25 × 2.5
Fukumoto et al. (2015)	John Hopkins, USA	1.5 T, SA	3.8/1.52	10~32	0.2 mmol/kg	1.3 × 1.3 × 2.0
Harrison et al. (2015a)	KCL, UK	1.5 T, PA	6.2/3.0	20	0.2 mmol/kg	1.3 × 1.3 × 4.0
Akoum et al. (2015)	DECAAF [†]	1.5 T; 3 T	5.2/2.4; 3.1/1.4	15	0.1~0.2 mmol/kg	1.25 × 1.25 × 2.5
Cochet et al. (2015)	Bordeaux, France	1.5 T, SA	6.1/2.4	15~30	0.2 mmol/kg	1.25 × 1.25 × 2.5

for automatic LA volume segmentation directly from LGE MRI (Xiong et al., 2020). Table 7 summarizes representative automatic LA segmentation methods and results from LGE MRI. The upper part of the table is the overview of conventional methods, while the bottom part summarizes DL-based methods.

In the conventional methods, many works incorporated anatomical or shape priors to improve the robustness against the large variability of LA shapes and intensity distributions. For example, Gao et al. (2010) used shape learning and region-based active contour evolution for LA segmentation. The shape learning was aimed to utilize prior shape knowledge, to solve the unclear boundary problem in LGE MRI when using the active contour method. Karim et al. (2010) adopted the Voronoi framework for the LA segmentation and optimized the model with a spatial and intensity prior in the form of a probabilistic atlas. Zhu et al. (2013) achieved the LA segmentation using a variational region growing with a moments-based shape prior. Nuñez-Garcia et al. (2018) constructed LGE MRI atlases via MAS and then clustered the LA shapes using principal component analysis (PCA) to perform a second MAS for the LA LGE MRI segmentation. In contrast to the studies of introducing shape priors, Tao et al. (2016a) combined LGE MRI with another MRI sequence with better anatomical information from the same patient for the LA segmentation of LGE MRI. Specifically, they first employed MAS to segment LA from the auxiliary MRI, and then mapped the generated label to LGE MRI followed by a level-set based local refinement. They compared the results of combining LGE MRI and auxiliary MRI with that of solely using LGE MRI (directly employing MAS on LGE MRI), and the combined version achieved better results. They also tested their method on the public dataset from the *Atrial Segmentation Challenge* where only LGE MRI sequence was provided (Qiao et al., 2018), and achieved better performance in terms of Dice compared to that in Tao et al. (2016a) (0.88 ± 0.03 vs. 0.86 ± 0.05). This may be due to the difference in the dataset, as the public data includes both pre- and post-ablation images. Similarly, Li et al. (2020b) employed an auxiliary MRI sequence to assist the LA segmentation of LGE MRI using a MAS method, and obtained better Dice score (0.898 ± 0.044) than these conventional methods. Particularly, Li et al. (2020b) and Nuñez-Garcia et al. (2018) adopted a multi-atlas based

whole heart segmentation (MA-WHS), and then extracted LA sub-structure. This is because LGE MRI generally covers the whole heart, and MA-WHS could be helpful to exclude surrounding sub-structures of LA.

In the DL-based approaches, both Chen et al. (2018b) and Li et al. (2020c) performed simultaneous LA and scar segmentation via multi-task learning. The simultaneous optimization scheme showed better performance than solving the two tasks independently, which ignored the intrinsic spatial relationship between LA and scars. Besides, Li et al. (2020c) introduced a spatial encoding (SE) loss to incorporate continuous spatial information of the LA. Their experiments showed that the SE loss could be effective to remove noisy patches in the final predicted segmentation, and therefore evidently reduced the Hausdorff distance (HD) value. Recently, many methods based on different network structures were developed with the launch of the *Atrial Segmentation Challenge* in MICCAI 2018. Jarmart et al. (2020) reviewed current state-of-the-art of DL approaches for LA segmentation from LGE MRI, where most reviewed papers were from the challenge event. Though most current methods employed U-Net as a baseline architecture, Jarmart et al. (2020) emphasized the importance of proper class imbalance management, suitable feature extraction procedure, and relevant loss function selection for the LA segmentation. Here, we will summarize all the DL-based methods from the participants of the challenge event and these used the dataset but did not participate in the event. Xiong et al. (2018) proposed an AtriaNet consisting of a multi-scale and dual pathway architecture, to capture both the local LA tissue geometry and the global positional information. They evaluated their algorithm on 154 LGE MRIs, and obtained average Dice scores of 0.940 ± 0.014 and 0.942 ± 0.014 for the LA epicardium and endocardium, respectively. Chen et al. (2018a) designed a two-task network for both LA segmentation and pre/post ablation image classification to learn additional anatomical information. The results indicated that multi-task learning obtained better segmentation performance compared to baseline U-Net method training with a single task. Besides, they employed a random gamma correction for contrast augmentation, to improve the robustness of the model for images with various image contrasts. Vesal et al. (2018) employed a 3D U-Net with dilated convolutions at the bottom of the network and residual connections

Table 7. Summary of previously published works on automatic LA volume/ geometry segmentation from LGE MRI. CNN: convolutional neural network; MAS: multi-atlas segmentation; MA-WHS: multi-atlas whole heart segmentation; SVM: support vector machine; KNN: K nearest neighbor; FCN: fully convolutional network; HAANet: hierarchical aggregation network; ASD: average surface distance; 95HD: 95% Hausdorff distance; VO: volume overlap; Jc: Jaccard; Acc: Accuracy; Se: Sensitivity; Sp: Specificity; Cf: Conform; APD: average perpendicular distance; Diam. Err: antero-posterior diameter error; Volume Err: volume error.

Study	Num	Pre/ Post	Algorithm	Evaluation	Dice _{LA}
Gao et al. (2010)	20	Post + Pre	Active contours + statistical shape learning	N/A	N/A
Karim et al. (2010)	30	Pre	Graph-cuts + Voronoi tessellation + probabilistic atlas	Overlap measure	N/A
Kutra et al. (2012)	59	Pre	Multi-model based fitting + SVM	Acc	N/A
Zhu et al. (2013)	64	Post + Pre	Variational region growing + shape prior	Dice, VO, 95HD, ASD	0.79 ± 0.05
Deng and Zhang (2016)	64	Post + Pre	KNN + super pixel voting	Dice, VO	0.81 ± 0.08
Tao et al. (2016a)	56	Pre	MAS + 3D level-set	Dice, ASD	0.86 ± 0.05
Núñez-García et al. (2018)	154	Post + Pre	MA-WHS + shape model	Dice, HD, ASD	0.842 ± 0.049
Qiao et al. (2018)	154	Post + Pre	MAS + level-set	Dice, APD	0.88 ± 0.03
Li et al. (2020b)	58	Post	MA-WHS	Dice	0.898 ± 0.044
Chen et al. (2018b)	100	Post + Pre	Multiview two-task network	Dice, Acc, Sp, Se	0.908 ± 0.031
Xiong et al. (2018)	154	Post + Pre	Dual CNNs	Dice, HD, Sp, Se	0.942 ± 0.014
Chen et al. (2018a)	154	Post + Pre	Multi-task 2D U-Net	Dice, Jc, HD, ASD	0.901 ± 0.003
Vesal et al. (2018)	154	Post + Pre	3D U-Net+ dilated + residual	Dice, Jc, Acc	0.926
Savioli et al. (2018)	154	Post + Pre	3D volumetric FCN	Dice, HD	0.851
Li et al. (2018a)	154	Post + Pre	Attention based 3D HAANet	Dice	0.923
Bian et al. (2018)	154	Post + Pre	ResNet101 + 2D pyramid Network	Dice, Cf, Jc, HD, ASD	0.929
Puybureau et al. (2018)	154	Post + Pre	VGG-16 + transfer learning + “pseudo-3D”	Dice	0.923
Liu et al. (2018)	154	Post + Pre	2D U-Net + FCN	Dice	0.903
Preetha et al. (2018)	154	Post + Pre	2D U-Net	Dice	0.888
de Vente et al. (2018)	154	Post + Pre	2D U-Net	Dice	0.897
Jia et al. (2018)	154	Post + Pre	Two-stage 3D U-Net + contour loss	Dice, HD, Sp, Se	0.907
Xia et al. (2018)	154	Post + Pre	Two-stage 3D V-net	Dice	0.932
Yang et al. (2018b)	154	Post + Pre	Two-stage 3D U-Net + transfer learning	Dice, Cf, Jc, HD, ASD	0.923
Borra et al. (2018)	154	Post + Pre	Otsu’s algorithm + 3D U-Net	Dice	0.898
Jamart et al. (2019)	154	Post + Pre	Two-stage 2D V-net	Dice, Jc, HD, ASD, Diam. Err, Volume Err	0.937
Yu et al. (2019)	100	Post + Pre	Uncertainty-aware model	Dice, Jc, 95HD, ASD	0.889
Wang et al. (2019a)	100	Post + Pre	Ensembled U-Net	Dice	0.921 ± 0.020
Du et al. (2020)	100	Post + Pre	Multi-scale dual-path network	Dice, Cf, Jc, HD	0.936 ± 0.005
Borra et al. (2020)	100	Post + Pre	2D/ 3D U-Net	Dice, HD, Sp, Se	$0.895 \pm 0.025/$ 0.914 ± 0.015
Li et al. (2020c)	60	Post	Multi-task 3D U-Net + spatial encoding	Dice, HD, ASD	0.913 ± 0.032

between encoder blocks, to incorporate both local and global knowledge. Li et al. (2018a) proposed an attention based hierarchical aggregation network (HAANet) for LA segmentation, and the basic network is a 3D U-Net. Instead of using U-Net or V-Net as the basic network, Bian et al. (2018) used ResNet101 for LA segmentation and adopted a pyramid module to learn multi-scale semantic information in feature map. Puybureau et al. (2018) achieved the LA segmentation by transfer learning from VGG-16, a pre-trained network used to classify natural images. Savioli et al. (2018) presented a 3D volumetric fully convolutional network (FCN) for LA segmentation. Liu et al. (2018), Preetha et al. (2018) and de Vente et al. (2018) all employed 2D U-Net for LA segmentation, and Liu et al. (2018) also tested the performance of FCN. Borra et al. (2020) tested both 2D and 3D U-Net for LA segmentation, and found that 3D pipelines showed significant better performance compared to the 2D pipelines. Jia et al. (2018), Xia et al. (2018), Yang et al. (2018b) and Jamart et al. (2019) all utilized two-stage U-Net/ V-Net and achieved top-performed results in the LA segmentation.

The first stage is to locate the region of interest (ROI), while the second stage is to perform detailed segmentation from the cropped ROI. Among them, Jia et al. (2018) proposed a novel contour loss function to include distance information for good shape consistency. Yang et al. (2018b) used transfer learning and dense deep supervision strategy to alleviate the risk of low training efficiency and potential overfitting. Instead of using the two-stage training strategy, Borra et al. (2018) applied the Otsu’s algorithm as a pre-processing to crop the ROI. Besides, Yu et al. (2019), Wang et al. (2019a) and Li et al. (2020c) all employed part of the dataset from the challenge event. Yu et al. (2019) proposed an uncertainty-aware self-ensembling model for semi-supervised LA segmentation. This is achieved by encouraging the segmentation to be consistent for the same input under different perturbations of the unlabeled data. Therefore, they could use abundant unlabeled data for training and obtained similar performance compared to the fully supervised methods using abundant labeled data. Wang et al. (2019a) utilized ensemble attention U-Net, dense U-Net and residual U-

Net models to segment LA. Du et al. (2020) adopted a dual-path structure network with multi-scale strategy for LA segmentation of LGE MRI.

In summary, conventional methods generally rely on the information from shape priors or an additional MRI sequence for accurate LA segmentation from LGE MRI. However, acquiring the auxiliary MRI requires extra work, and may introduce further errors, i.e., misalignment between LGE MRI and the auxiliary MRI. Recently, with the development of DL and release of public data, many methods could directly segment LA from LGE MRI, and achieved promising results. However, there still exist large errors in the PV and MV regions. This is mainly due to the small size, the large variability of PVs, including the number, position and orientation of the PVs, and the unclear boundary of MV. Note that PVs are crucial structures for AF analysis, as scars and ablation gaps are mainly located around PVs after PVI procedures. To improve the performance of DL-based methods, multi-task learning is effective, and a two-stage network is also a recommended training strategy as it could alleviate the class imbalance issue. It is also important to include shape prior or spatial information into the DL-based framework for robust LA segmentation, especially when the training data is limited. Besides, the accuracy of LA segmentation was found to be correlated to the image quality of LGE MRI (Pearson's correlation = 0.38) (Xiong et al., 2020). It is interesting that the reviewed methods show that 2D and 3D CNN had comparable performance, though the target LGE MRI belongs to 3D image.

3.2. LA wall segmentation

To the best of our knowledge, there are only few works for automatic LA wall segmentation in the literature, especially from LGE MRI. Many works estimated LA wall from LGE MRI just as an initialization step for scar segmentation (Karim et al., 2013; Yang et al., 2018a; Wu et al., 2018), and they will not be included in this review. This is because most of these works simply dilated the generated LA endocardium by assuming a fixed wall thickness for approximated LA wall segmentation (Karim et al., 2013). However, LA wall thickness varies with positions of the same patient and patients with different gender, age and disease status (Pan et al., 2008). With the wall segmentation, the wall thickness could be accurately calculated. For the review of existing techniques of wall thickness measurement, one can refer to Table 1 of the benchmark paper by Karim et al. (2018). *Considering the limited number of works reported on the LA wall segmentation task, in this section we will also include the reviews on other modalities, such as non-enhanced MRI and CT.* Table 8 summarizes the representative automatic LA wall segmentation methods and results from (LGE) MRI and CT.

With LGE MRI, Hsing et al. (2014) manually measured the wall thickness. Veni et al. (2017) proposed a shape-based generative model namely ShapeCut, to extract epicardial and endocardial surfaces for the LA wall segmentation from LGE MRI. The model could incorporate both local and global shape priors within a maximum-a-posterior estimation framework, and the shape parameters could be optimized via graph-cuts algorithm. Zhao et al. (2017) calculated the wall thickness by solving the Laplace equations on both epicardial and endocardial

surfaces. Wang et al. (2019b) employed the multi-planar convex hull approach to extract the epicardial and endocardial surfaces, and then used the coupled partial differential equations (PDE) for the wall thickness measurement. Compared to ex vivo data, they observed that wall thickness values in LGE MRI were more difficult to measure and validate. Besides, there was a discrepancy in wall thickness between ex vivo data and LGE MRI. Specifically, the wall thickness values measured from ex vivo data were consistently higher than those measured in LGE MRI.

With non-enhanced MRI, Karim et al. (2018) presented the LA wall segmentation and thickness measurement results from three conventional methods, i.e., level-set, region growing and watershed. The results showed that level-set performed evidently better than other two methods. Especially, region growing generally over-estimated thickness and performed poorly in the wall segmentation task. Overall, algorithms performed worse in MRI than in CT.

With CT, Inoue et al. (2014) employed a multi-region segmentation software to segment the LA blood pool and wall, and then manually corrected the regions that misclassified into blood pool. Bishop et al. (2016) adopted morphological operations on the segmented blood pool for wall segmentation, and then solved the Laplace equations over a finite element mesh of the LA to measure the wall thickness. In the benchmark paper (Karim et al., 2018), three algorithms for LA wall segmentation of CT were summarized. More specifically, Inoue and Drangova (2016) segmented the LA wall using the mesh vertex normal traversal method, where the mesh was constructed from the provided manual LA segmentation. Tao et al. (2016b) first employed nonlinear intensity transformation to enhanced LA wall region considering the limited soft tissue contrast in CT. Then, they used the level-set approach to extract the inner and outer LA surface for the final wall segmentation. Jia et al. (2016) adopted the region growing method for endocardial segmentation, and then utilized Marker-controlled geodesic active contour for epicardial segmentation.

In summary, currently reported LA wall segmentation works were all based on the conventional methods, including level-set, active contour, region growing, watershed and graph-cuts. To the best of our knowledge, no DL-based method has been applied to LA wall segmentation yet. This might be due to the limited relevant public datasets and large inter- and intra-observer variations of the manual segmentation. As Karim et al. (2018) reported, a common error of LA wall segmentation is from the surrounding tissue such as the neighbouring aortic wall. Improving the image quality could mitigate this problem, and active contour methods with shape constraints and level-set approaches could also be helpful. One of the main application of LA wall segmentation is to measure wall thickness. However, most of the reported algorithms rely on ruler-based assessments via digital callipers instead of performing a prior segmentation of the LA wall (Karim et al., 2018). Few works employed Laplace equation or PDE to measure wall thickness after achieving LA wall segmentation. Karim et al. (2018) demonstrated that their proposed wall thickness atlas could be effective for thickness prediction in new cases via atlas prop-

Table 8. Overview of previously published works on LA wall segmentation from CT and (LGE) MRI. MSE: mean square error; A: anterior; P: posterior; Tk: thickness; GAC: geodesic active contour; PDE: partial differential equations. Note that the evaluation measures and results in Inoue and Drangova (2016), Tao et al. (2016b) and Jia et al. (2016) are from the benchmark paper Karim et al. (2018).

Study	Data	Algorithm	Evaluation	Result
Hsing et al. (2014)	55 LGE MRI	Manual	Tk	Tk = 7.0 ± 1.8 mm (before ablation) Tk = 10.7 ± 4.1 mm (after ablation)
Veni et al. (2017)	72 LGE MRI + 170 Synthetic	ShapeCut	ASD, HD, clinical evaluation	Synthetic: ASD = 0.25 ± 0.04 mm; HD = 1.95 ± 0.38 mm LGE MRI: ASD = 0.66 ± 0.14 mm LGE MRI scar segmentation: MSE = 3.07; R-square = 0.83
Zhao et al. (2017)	LGE MRI	Laplace equation	Tk	Tk = 3.7 ± 1.7 mm
Wang et al. (2019b)	154 LGE MRI + ex vivo data	Convex hull method + coupled PDE	Tk	LGE MRI: Tk = $0.4\text{--}11.7$ mm and median = 3.88 mm
Karim et al. (2018)	10 MRI	Level-set	Tk, Dice, tissue mass	Tk = 2.16 ± 0.58 mm, Dice = 0.72
		Region growing		Tk = 6.04 ± 3.63 mm, Dice = 0.39
		Watershed		Tk = 3.45 ± 3.57 mm, Dice = 0.67
Inoue et al. (2014)	5 enhanced CT	Multi-region segmenta- tion software + manual correction	Tk, visualization	Tk = 0.5–3.5 mm
Bishop et al. (2016)	10 CT	Morphological operations + Laplace equation	Tk	Errors ≤ 0.2 mm for Tk of 0.5–5.0 mm
Inoue and Dran- gova (2016)	10 CT	Mesh vertex normal traversal	Tk, Dice, tissue mass	Tk = 1.13 ± 1.02 mm (A), 1.26 ± 0.83 mm (P) Dice = 0.33 (A), 0.39 (P)
Tao et al. (2016b)	10 CT	Nonlinear intensity trans- formation + level-set	Tk, Dice, tissue mass	Tk = 1.34 ± 0.89 mm (A), 0.78 ± 0.41 mm (P) Dice = 0.43 (A), 0.21 (P)
Jia et al. (2016)	10 CT	Region growing + Marker-controlled GAC	Tk, Dice, tissue mass	Tk = 0.75 ± 0.38 mm (A), 1.46 ± 1.57 mm (P) Dice = 0.30 (A), 0.50 (P)

agation. They constructed a flat thickness map via a surface flattening and unfolding strategy, to compare the mean thickness in each sub-region of LA wall. Finally, though CT is the optimal modality for imaging the thin wall owing to its high resolution, MRI could be effective to assess the wall tissue viability. Therefore, much greater attention needs to be given to the LA wall segmentation from MRI, especially LGE MRI.

3.3. LA scar segmentation and quantification

In the literature, only a small number of works have been reported targeting the fully automatic segmentation or quantification of LA scars, to the best of our knowledge, and most of the methods require an accurate manual segmentation of LA cavities or LA walls, as an initialization, for following steps of scar classification. For example, the *Atrial Segmentation Challenge* (Rhode and Karim, 2012) provided LA labels for participants to develop scar segmentation algorithms. Eight research teams contributed their methods to this task, including histogram analysis, threshold, k-means clustering, region-growing with EM-fitting, active contour and graph-cuts (Karim et al., 2013). The benchmark study showed that the performance of semi-automatic methods initialized with manual LA wall segmentation were better than fully automatic approaches (Karim et al., 2013). Currently, the most commonly used approach for LA scar segmentation is based on thresholding (Pontecorboli et al., 2017). The threshold value is normally defined by assuming a fixed standard deviations (SD) above the average intensity value of a normal wall region or blood pool (Oakes et al., 2009; Badger et al., 2010; Ravanelli et al., 2014). For details,

one can refer to the work by Pontecorboli et al. (2017), who reviewed and compared different thresholding-based scar segmentation techniques. These methods are easy-to-implement and intuitive, but also have disadvantages. Firstly, the setting of threshold values is subjective, and the values can differ significantly across different scans, due to difference of timing from gadolinium administration (Karim et al., 2014; Chubb et al., 2018). Secondly, the accuracy of scar segmentation highly relies on the accuracy of LA or LA wall segmentation, which is also challenging and could only be achieved via semi-automatic or manual approaches (Oakes et al., 2009; Badger et al., 2010). Therefore, other schemes have been developed. Table 9 summarizes all the works, where conventional methods are listed in the upper part and DL-based algorithms are enumerated in the bottom part.

In the conventional techniques, instead of using thresholding, Knowles et al. (2010) and Tao et al. (2016a) employed maximum intensity projection (MIP) to quantify scars on the LA surface. The projection range should be selected carefully, namely it needs to be large enough to extend into the LA myocardium, but not too far to include the intensity of other positions. Knowles et al. (2010) and Tao et al. (2016a) performed at ± 3 mm and ± 2 mm along each normal vector of the LA surface respectively, to consider the potential errors of LA segmentation. Karim et al. (2011) proposed a probabilistic tissue intensity model which was formulated as Markov random field and solved using graph-cuts. In their following work (Karim et al., 2014), they presented a scar quantification method by combining the scar intensity model priors and Gaus-

Table 9. Summary of previously published works on (semi-)automatic *LA fibrosis/ scar segmentation and quantification* from LGE MRI. ~M Post: ~months post-ablation; Pre: pre-ablation; XOR: XOR overlap; Percentage: scar percentage; RMSE: root MSE; Volume: total scar volume; ROC: receiver operating characteristic; BER: balanced error rate; FCC: fuzzy c-means clustering; MIP: maximum intensity projection; GMM: Gaussian mixture model; SSAE: stacked sparse auto-encoders; MS-CNN: multi-scale CNN; EAM-c: correlation with electroanatomical mapping. Here, the asterisk (*) indicates the method employed manual LA wall segmentation.

Study	Num	Pre/ Post	Algorithm	auto?	Evaluation	Dice _{scar}
Oakes et al. (2009)	81	Pre	2–4 SD	semi-auto	Percentage, EAM-c	N/A
Badger et al. (2010)	144	3–20M Post	3 SD	semi-auto	Percentage, EAM-c	N/A
Knowles et al. (2010)	7	Post + Pre	MIP	semi-auto	Percentage, EAM-c	N/A
Karim et al. (2011)	9	6M Post	Probabilistic intensity model	auto	Percentage	N/A
Perry et al. (2012)	34	3M Post	K-means clustering	semi-auto	Dice, XOR, Percentage	0.807 ± 0.106
Karim et al. (2013)	60	Post + Pre	Hysteresis threshold	semi-auto	Dice, RMSE, Volume	0.76 ^{post} ; 0.37 ^{pre}
	60	Post + Pre	Region growing + EM-fitting			0.85 ^{post} ; 0.22 ^{pre}
	40	Post + Pre	Graph-cuts + FCC			0.73 ^{post} ; 0.17 ^{pre}
	15	Post	Active contour + EM-fitting			0.76 ^{post}
	30	Post + Pre	Simple threshold*			0.84 ^{post} ; 0.48 ^{pre}
	60	Post + Pre	Graph-cuts			0.78 ^{post} ; 0.30 ^{pre}
	60	Post + Pre	Histogram analysis + threshold*			0.78 ^{post} ; 0.42 ^{pre}
	60	Post + Pre	K-means clustering*			0.72 ^{post} ; 0.45 ^{pre}
	60	Post + Pre	2 SD			0.58 ^{post} ; 0.24 ^{pre}
	60	Post + Pre	3 SD			0.17 ^{post} ; 0.16 ^{pre}
	60	Post + Pre	4 SD			0.14 ^{post} ; 0.31 ^{pre}
	30	1–6M Post	6 SD			0.35 ^{post}
Ravanelli et al. (2014)	60	Post + Pre				0.59 ^{post} ; 0.05 ^{pre}
	10	Pre	4 SD	semi-auto	Dice, EAM-c	0.600 ± 0.210
	15	6M Post	GMM + graph-cuts	semi-auto	Dice, ROC, Volume	> 0.8
	46	Pre	MIP	auto	Qualitative visualization	N/A
	72	Post + Pre	K-means clustering	auto	Percentage	N/A
Yang et al. (2018a)	37	Post	Super-pixel + SVM	auto	Dice, Acc, Se, Sp, ROC, BER	0.790 ± 0.050
Wu et al. (2018)	36	Post	Multivariate mixture model	auto	Dice, Acc, Se, Sp	0.556 ± 0.187
Yang et al. (2017b)	20	Post + Pre	Super-pixel + SSAE	auto	Dice, Acc, Se, Sp, ROC	0.776 ± 0.146
Li et al. (2018b)	100	Post + Pre	Graph-cuts + CNN	auto	Dice, Acc, Se, Sp	0.566 ± 0.140
Chen et al. (2018b)	100	Post + Pre	Multiview two-task network	auto	Dice, Acc, Se, Sp, Percentage	0.78 ± 0.08
Yang et al. (2020)	190	Post + Pre	Multiview two-task network	auto	Dice, Acc, Se, Sp	0.870
Li et al. (2020b)	58	6M Post	Graph-cuts + MS-CNN	auto	Dice, Acc, Se, Sp, GDice	0.702 ± 0.071
Li et al. (2020a)	60	3–27M Post	Multi-task network	auto	Dice, Acc, GDice	0.543 ± 0.097

sian mixture model (GMM). Besides, they added smoothness constraints via the graph-cuts approach to ensure smoothness and avoided discontinuities in the final scar segmentation. The proposed method was evaluated on both numerical phantoms and clinical datasets, and demonstrated a good concordance between the automatic results and manual delineations. Here, numerical phantoms could offer a wide range of variation in scar contrast, which is usually unavailable in clinical datasets. Perry et al. (2012) employed k-means clustering to segment scars from manually segmented LA wall region. As mentioned before, the benchmark paper (Karim et al., 2013) compared eight methods with the full-width-at-half-maximum (FWHM) and n -SD methods, which all employed manual LA segmentation as an initialization, and three of them further utilized manual LA wall segmentation. Among the eight methods, region growing with EM-fitting method obtained the best performance for post-ablation dataset in terms of Dice, even better than those methods that directly employed manual LA wall segmentation

for initialization. For pre-ablation data, the three methods with a manual LA wall initialization achieved evidently better Dice compared to other five methods only with a manual LA initialization. In general, all the evaluated eight methods in the benchmark paper outperformed the FWHM and n -SD methods. Note that both the SD and FWHM required an experienced observer to identify an enhanced/ normal region within LA wall, so results could vary with a different selections. Besides, Karim et al. (2013) classified the LGE MRI into three types, i.e., good, average and poor, according to its SNR and CR for scars. They found that most methods had a marginally lower Dice on scans with worse quality, but without statistical significance. This could be because the quality difference is minor, and the accurate initialization of manual LA segmentation also alleviated the effect of poor image quality. Veni et al. (2017) used the same k-means clustering method as Perry et al. (2012), but the LA wall was automatically segmented by their proposed Shape-Cut method. Yang et al. (2018a) employed super-pixel to over

segment scars and then utilized the support vector machine algorithm to classify the over-segmented super-pixels into scar-ring and normal wall regions. They scored the image quality into 0 (non-diagnostic), 1 (poor), 2 (fair), 3 (good) and 4 (very good) on a Likert-type scale, according to the level of SNR, appropriate T1 and the existence of navigator beam and ghost artefacts. Due to the poor image quality of the dataset, only subjects with image quality ≥ 2 were selected into their study for evaluation. Wu et al. (2018) combined LGE MRI with anatomical MRI for scar quantification based on the multivariate mixture model (MvMM) and maximum likelihood estimator (MLE). They formulated a joint distribution of images using the MvMM (Zhuang, 2019), where the registration of the two MRIs and scar segmentation of LGE MRI were performed simultaneously. Then, the transformation and model parameters were optimized by the iterated conditional model algorithm within the MLE framework.

For the DL-based works, Yang et al. (2017b) employed a DL-based classifier for automatic LA scar segmentation. They used super-pixel over-segmentation for feature extraction, and then adopted a supervised classification step via stacked sparse auto-encoders. However, they only used handcrafted intensity features, which consisted of limited information. In contrast, Li et al. (2018b) proposed a hybrid approach utilizing a graph-cuts framework combined with CNNs to predict edge weights of the graph for automatic scar segmentation. They extended their work by introducing multi-scale CNN (MS-CNN) to learn local and global features simultaneously (Li et al., 2020b). The experiment shows that the multi-scale learning scheme (number of scales = 3) improved the performance compared to the method with single-scale (Dice_{scar}: 0.702 ± 0.071 vs. 0.677 ± 0.070). Besides, the scheme also contributed to the less demanding of the accurate LA segmentation, and therefore made the scar segmentation to be more robust. A major limitation of this study is the lack of an end-to-end training style, as the framework was split into three sub-tasks, i.e., LA segmentation as an initialization, feature learning via the MS-CNN and optimization based on graph-cuts. This is mainly because the proposed multi-scale patch strategy led to an expensive time and space complexity, which made the end-to-end training on the whole graph to be infeasible. In the subsequent study, they developed a new framework where LA segmentation, scar projection onto the LA surface, and scar quantification are performed simultaneously in an end-to-end fashion (Li et al., 2020a). In this framework, they proposed a shape attention (SA) mechanism by an implicit surface projection, to utilize the inherent spatial relationship between the LA cavity and scars. The mechanism also alleviated the class-imbalance problem in the scar quantification, and proved to be effective in the ablation study. Similarly, Chen et al. (2018b) and Yang et al. (2020) adopted multi-task learning for simultaneous LA and scar segmentation, but the spatial relationship between the two regions were not explicitly learned in their works.

In summary, the scar segmentation/ quantification from LGE MRI remains an open problem. Most methods relied on interactive correction, manual initialization, or simply employed subjective thresholding. These semi-automatic approaches gen-

erally obtained high accuracies in terms of Dice scores. Compared to the conventional automatic methods, DL-based algorithms could obtain better performance. However, DL-based models generally have limited model generalization ability. In general, pre-ablation data with fibrosis is more challenging to segment than post-ablation data with scars. This may be because fibrosis appears more diffuse compared to post-ablation scars (Karim et al., 2013). In addition, it is difficult to differentiate the native fibrosis and post-ablation scars for long-standing persistent AF patients (Yang et al., 2017a). One major challenge for scar segmentation/ quantification is the artifacts from the boundary regions, such as from the right atrial (RA) wall and aorta wall. A good initialization, i.e., accurate LA or LA wall segmentation, could be helpful to counteract this problem. Li et al. (2020b) tried to reduce the dependence on the accurate LA segmentation via projection and MS-CNN, while Li et al. (2020a) achieved this by learning spatial information of LA based on distance transform maps. Another challenge arises from the imaging, including poor image quality and data-mismatch issues in DL-based methods. Therefore, a more consistent and standard image acquisition protocol is highly required. Alternatively, domain generalization algorithms need to be considered to improve the model generalization ability across different sites or on unseen datasets (Li et al., 2021).

3.4. LA ablation gap quantification

Gaps around PVs can be classified into electrical/ conduction gaps and anatomical ablation gaps. Conduction gaps refer to the electrical reconnection regions with high voltages in the electroanatomical mapping (EAM), and they can be detected using intra-cavitary catheters during a redo procedure. Ablation gaps indicate the healthy tissue regions in the (ideally continuous) scars, which are typically identified by LGE MRI. Therefore, in this section, we only focus on the developed methods to quantify ablation gaps from LGE MRI. To the best of our knowledge, most of the methods reported in literature relied on visual inspection, which could result in biased estimations of gap characteristics, such as the number, length and position of gaps.

Table 10 summarizes representative (semi-)automatic LA ablation gap quantification methods, results and main findings. Badger et al. (2010) and Mishima et al. (2019) both employed thresholding for scar segmentation, and then detected ablation gaps in visual. Ranjan et al. (2012) and Harrison et al. (2015a) both utilized software for gap quantification, i.e., *Osirix* and Custom-written software, respectively. Besides, Ranjan et al. (2012) found that real time MRI system can be employed for gap quantification. Bisbal et al. (2014) manually segmented the LA wall for an accurate initialization and then adopted MIP for scar and gap classification. Linhart et al. (2018) used the image intensity ratio (IIR) as a threshold for scar segmentation, and defined the gaps as the discontinued ablation line ≤ 3 mm. Recently, Nuñez-García et al. (2019) proposed a reproducible framework for gap quantification using a graph-based method. The accuracy of these methods generally depends on the prior step of LA segmentation. Also, a fixed regional parcellation is generally assumed, i.e., four-PV configuration in the LA, but

Table 10. Summary of previously published works on (semi-)automatic *ablation gap quantification* from LGE MRI. # gaps: mean number of gaps; GL: gap length; IIR: image intensity ratio; NAUC: normalised area under the curve; RSPV: right superior PV; LIPV: left inferior PV; LSPV: left superior PV.

Study	Num	Algorithm	Evaluation	Results & Main findings
Badger et al. (2010)	144	3 SD for scar segmentation + visually detect gap	Visual, EAM-c	Significant relationship between gaps and recurrence; Achieving complete circumferential lesions around the PV is difficult.
Ranjan et al. (2012)	12	Measurement tool in <i>Osirix</i>	GL, pathology correlation	The correlation coefficient (R^2) between the GL identified by LGE MRI and the gross pathology was 0.95; GL = 1.0 mm (via gross pathology) and GL = 1.4 mm (via LGE MRI); Real time MRI system can be used to identify gaps.
Bisbal et al. (2014)	50	Manual LA wall + MIP	GL, # gaps, EAM-c	# gaps = 4.4/patient; # gaps = 1.27 ± 0.41 /PV Median GL = 13.33 ± 5.8 mm/gap; Position of highest # gaps: RSPV (=1.53); Position of fewest # gaps: LIPV (=0.67); The majority of patients (73.3%) had gaps in all PVs. LGE MRI may identify non-conducting gaps that could be related to later recurrences.
Harrison et al. (2015a)	20	Custom-written software	Visual, EAM-c	Weak point-by-point relationship ($R^2=0.57$) between scars and endocardial voltage in patients undergoing repeat LA ablation; The mean voltage within scar region is lower than that within normal wall region.
Linhart et al. (2018)	94	IIR for scar segmentation + gap is defined as discontinuation of the ablation line by ≤ 3 mm	GL, # gaps, EAM-c	# gaps = 5.4/patient; Mean GL = 7.3 mm/gap; 90 out of 94 patients (96%) had at least 1 anatomic gap; Anatomic gaps are frequently detected in LGE MRI at 3 months after first PVI; An increase of 10% relative GL increased the likelihood of AF recurrence by 16%; The total relative GL was significantly associated with recurrence instead of # gaps.
Mishima et al. (2019)	10	2 SD for scar segmentation + visually detect gap	GL, # gaps, EAM-c	Mean GL = 11.6 ± 3.9 mm/gap; # gaps = 1.6/patient (1st ablation); # gaps = 1.4/patient (2nd ablation); Position of highest # gaps: RSPV (=2); Position of fewest # gaps: LIPV (=0); The location of electrical gaps are well matched to that on the LGE MRI.
Núñez-García et al. (2019)	50	Graph-based method	GL, # gaps, RGM	Position of highest # gaps: LSPV (=1.73); Position of fewest # gaps: LIPV (=1.16); No significant differences between left and right PVs; No significant relationship between gaps and recurrence.

actually only around 70% LA have four PVs (Prasanna et al., 2014).

It is considered difficult to achieve complete circumferential lesions, so the majority of patients had gaps after ablation (Badger et al., 2010; Bisbal et al., 2014; Linhart et al., 2018). The most common locations appearing gaps are the area between the left superior PV (LSPV) and the LAA. This may be due to the presence of a thicker myocardium in this area, which leads to non-transmural lesions (Galand et al., 2016). In (Bisbal et al., 2014; Mishima et al., 2019), the largest number of gaps occurred in right superior PV (RSPV) was reported; while in (Núñez-García et al., 2019) it was occurred in LSPV. In contrast, the fewest of gaps occurred consistently in the left inferior PV (LIPV) (Bisbal et al., 2014; Mishima et al., 2019; Núñez-García et al., 2019). The different distributions of gaps in different PV positions could be attributed to the differences of imag-

ing and limited accuracy of scar segmentation of these regions.

The relationship between electrical gaps of the EAM and anatomical gaps of the LGE MRI is still unclear. Mishima et al. (2019) found that the location of electrical gaps are well matched to that of the detected ablation gaps from LGE MRI. However, Harrison et al. (2015a) claimed a weak point-by-point relationship between scars and EAM in the patients with repeat LA ablation. Besides, the relationship between ablation gaps and AF recurrence is also controversial, with positive answers (Peters et al., 2009; Taclas et al., 2010; Badger et al., 2010; Bisbal et al., 2014; Linhart et al., 2018) but also negative conclusions (Spragg et al., 2012; Harrison et al., 2015b; Núñez-García et al., 2019). These are partially due to the lack of an objective and consistent method for ablation gap quantification, primarily depending on visual observation. The task has not been properly addressed in the literature, and research on this is still at an

early stage.

4. Data and evaluation measures

Validation work not only reveal the performance and limitations of a proposed method, but also clarify the scope of its application (Jannin et al., 2006). Hence, it is essential to validate an algorithm before applying it to a clinical setting. This section examines and analyzes the validation methods used for each aforementioned task in the literature, including the data and performance measures. We also focus on the evaluation of clinically relevant measures, besides the evaluation of computing accuracy of the algorithms.

4.1. Data

For LA segmentation, Zhao and Xiong (2018) organized the *Atrial Segmentation Challenge*, which provided a platform with 154 public LGE MRIs for evaluating and comparing current and future works in the field. For LA wall segmentation, Karim and Rhode (2016) organized the *Left Atrial Wall Thickness Challenge*, where they provided 10 CT and 10 non-enhanced MRI images, and Utah (2012) released a public LGE MRI dataset with manual segmentation of LA walls. Note that though Zhao and Xiong (2018) also provided LA wall segmentation, it was actually generated using the morphological (dilation) operation from the LA segmentation results.

Besides LGE MRI, synthetic and ex vivo data were employed for LA wall segmentation and wall thickness measurement. Here, synthetic images were simulated without using a real scanner, so users could control all image parameters and easily obtain the ground truth. For scar segmentation and quantification, two public datasets were employed for validation, i.e., the dataset from Rhode and Karim (2012) and Utah (2012). Currently, public datasets for gap quantification and evaluation are not available, to the best of our knowledge.

4.2. Evaluation measures

4.2.1. LA cavity measures

For assessing the performance of LA cavity segmentation, a range of different measures have been explored, as shown in Table 7. The most widely used measures include the Dice coefficient/ score, Jaccard index, (95)HD, and average surface distance (ASD). They are defined as follows,

$$\text{Dice}(V_{\text{auto}}, V_{\text{manual}}) = \frac{2|V_{\text{auto}} \cap V_{\text{manual}}|}{|V_{\text{auto}}| + |V_{\text{manual}}|}, \quad (1)$$

$$\text{Jaccard}(V_{\text{auto}}, V_{\text{manual}}) = \frac{|V_{\text{auto}} \cap V_{\text{manual}}|}{|V_{\text{auto}} \cup V_{\text{manual}}|}, \quad (2)$$

$$\text{HD}(X, Y) = \max \left[\sup_{x \in X} \inf_{y \in Y} d(x, y), \sup_{y \in Y} \inf_{x \in X} d(x, y) \right], \quad (3)$$

and

$$\text{ASD}(X, Y) = \frac{1}{2} \left(\frac{\sum_{x \in X} \min_{y \in Y} d(x, y)}{\sum_{x \in X} 1} + \frac{\sum_{y \in Y} \min_{x \in X} d(x, y)}{\sum_{y \in Y} 1} \right), \quad (4)$$

where V_{manual} and V_{auto} denote the manual and automatic segmentation, respectively; X and Y represent two sets of contour points; $d(x, y)$ indicates the Euclidean distance between the two points x and y ; and $|\cdot|$ refers to the number of pixels. Dice and Jaccard are selected for volumetric overlap measurement, where Jacquard index can be more sensible and severe upon small variation compared to Dice (Jamart et al., 2019). ASD and HD are used to evaluate the shape and contour accuracy of the LA. ASD calculates the average of the distances between all pairs of pixels between two surfaces. HD calculates the largest error distance of the 3D segmentation defined for a prediction of LA volume. Therefore, HD can further measures the existence of outlier.

In addition, three statistical measurements are employed, i.e., Accuracy (Acc), Specificity (Sp), and Sensitivity (Se), defined as follows,

$$\text{Acc} = \frac{TP + TN}{TP + FP + FN + TN}, \quad (5)$$

$$\text{Sp} = \frac{TN}{TN + FP}, \quad (6)$$

and

$$\text{Se} = \frac{TP}{TP + FN}, \quad (7)$$

where TP , TN , FN and FP stand for the number of true positives, true negatives, false negatives and false positives, respectively. Acc represents the proportion of true results (both TP and TN) among the total number of cases examined. Sp and Se are used to reflect the success of the algorithm for the foreground (LA cavity) and the background segmentation, respectively. Besides, the diameter and volume error calculations are used to assess the medical relevance of the automatic reconstructed LA volumes in clinic.

4.2.2. LA wall measures

For LA wall segmentation, wall thickness and Dice are currently the most commonly used measures. The thickness (Tk) of the LA wall can be calculated by averaging the thickness over each pixel $p_i \in S_{\text{epi}}$ from the epicardium S_{epi} to the endocardium S_{endo} , and therefore is defined as,

$$\text{Tk} = \frac{\sum_{p_i \in S_{\text{epi}}} d(p_i, S_{\text{endo}})}{|S_{\text{epi}}|}. \quad (8)$$

Actually, when the object size is far smaller than the background (as in the case of the LA wall), overlap-based metrics based on the four overlap cardinalities (TP, TN, FP, FN) are generally inappropriate (Taha and Hanbury, 2015). This is because they will provide the same metric value, regardless of the distance between two non-overlapping regions evaluated, ultimately affecting the objectivity in precision. Therefore, both Dice and Jaccard are not suitable since they can also be represented as,

$$\text{Dice} = \frac{2TP}{2TP + FP + FN}, \quad (9)$$

$$\text{Jaccard} = \frac{TP}{TP + FP + FN}. \quad (10)$$

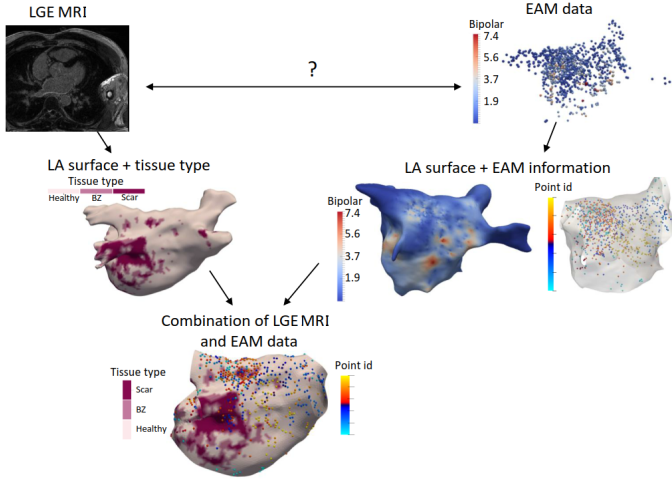


Fig. 6. The spatial correspondence of LGE MRI and EAM data. Image adopted from Núñez García et al. (2018).

In this case, distance based metrics are recommended, as they consider the precision and accuracy of both the shape and local alignment of segmented regions. Apart from its small size, the LA wall is also accompanied by adjacent PV structures, which also exhibit large inter-observer variation and could be regarded as outliers since they actually do not belong to LA wall. Compared to HD which is sensitive to outliers, ASD is a better option for LA wall quantitative assessment. As the LA wall segmentation involves the two surfaces, i.e., the epicardium and endocardium, the ASD of the LA wall is defined as,

$$ASD_{wall} = \max \{ASD_{epi}, ASD_{endo}\}. \quad (11)$$

Apart from these measurements, tissue mass and clinical evaluation are also employed for LA wall segmentation evaluation. The tissue mass M is designed to predict the volume error, and the difference in mass is defined as,

$$\Delta M = \rho \times |V - \hat{V}|, \quad (12)$$

where $\rho = 1.053 \text{ g/ml}$ (Vinnakota and Bassingthwaite, 2004) is the average wall tissue density, and V and \hat{V} refer to the ground truth and predicted volume, respectively (Karim et al., 2018). Furthermore, Veni et al. (2017) proposed to compare the scar percentages within the manually and automatically segmented LA wall. The basic idea behind this is that the LA wall segmentation is usually regarded as an initial step for scar segmentation as mentioned earlier.

4.2.3. LA scar measures

The optimal evaluation method to quantify scars from LGE MRI is still controversial due to the lack of ground truth. Currently, the EAM system is regarded as the clinical standard technique for scar assessment, as presented in Fig. 6. The widely used bipolar voltage threshold defining the LA scars is $\leq 0.05 \text{ mV}$, which has been propagated through the literature and clinical practice (Harrison et al., 2014). However, the correlation between the LA scars identified by LGE MRI (enhanced regions) and EAM (low voltage regions) is still being questioned.

The subjective and inaccurate scar segmentation might be one of the main reasons.

Alternatively, most algorithms employ manual segmented LA scars as the ground truth. For this evaluation, volume overlap measures and scar percentage are commonly used, as Table 9 shows. For example, Perry et al. (2012) proposed a novel overlap measure for scar evaluation, namely XOR overlap,

$$XOR(V_{auto}, V_{manual}) = \frac{|W| + |V_{auto} \oplus V_{manual}|}{|W|}, \quad (13)$$

where $|W|$ is the set of voxels belong to the LA wall, and \oplus refers to exclusive OR. The XOR overlap measure emphasizes the difference between overlapping scars, and will not be affected by the size of scars.

However, as mentioned in Section 4.2.2 volume overlap measures (such as Dice) could be highly sensitive to the mismatch of small structures (namely scars here), so in instances it will impose disproportionate penalties on the algorithm. To mitigate the effect of small size of scars, Li et al. (2020b) proposed to project the appearance of scars onto the LA surface for both ground truth and automatic segmentation results, and then calculate the Dice scores of scars on the projected LA surface instead of on the 3D volume (Wu et al., 2018; Li et al., 2018b, 2020b,a). Furthermore, Li et al. (2020b,a) computed the generalized Dice (GDice) of scars from the projected LA surface for more interpretation. GDice is defined as follows,

$$GDice = \frac{2 \sum_{k=0}^{N_k-1} |S_k^{auto} \cap S_k^{manual}|}{\sum_{k=0}^{N_k-1} (|S_k^{auto}| + |S_k^{manual}|)}, \quad (14)$$

where S_k^{auto} and S_k^{manual} indicate the segmentation results of label k from the automatic method and manual delineation on the LA surface, respectively, N_k is the number of labels, and $N_k = 2$ here to represent scarring ($k = 1$) and normal wall ($k = 0$) regions.

Karim et al. (2013) proposed a surface-based metric, which employed MIP to calculate the distance error between the mesh vertex points on the LA surface. The distance error is defined as the root mean squared error (RMSE), i.e.,

$$RMSE = \sqrt{\frac{1}{N} \sum_{i=1}^N d(v_i^{auto}, v_i^{manual})^2}, \quad (15)$$

where v_i^{auto} and v_i^{manual} are the set of mesh vertices belonging to scars from the prediction and ground truth, respectively. The major limitation of the surface based metric is that targets with a significant amount of FP scars will have a low RMSE error. Nevertheless, it can be overcome by combining the surface measure with a volume-based index.

Scar percentage is directly related to clinical categorization of AF patients, according to Table 1, and thus should be appropriate as an assessment measure. Besides, one could analyze the relationship of scar percentages between manually and automatic scar segmentation, to evaluate the performance of automatic scar segmentation. For example, Veni et al. (2017) quantified the scar percentage correlation using the mean square error (MSE) and R-square value. Many works also calculate the

volume error of scars for evaluation, which is defined as,

$$\delta V = |V_{auto} - V_{manual}|. \quad (16)$$

Statistical measurements related to scar classification could be employed for evaluation, including Acc, Se, Sp, receiver operating characteristic (ROC) curve, and balanced error rate (BER).

4.2.4. LA ablation gap measures

As Table 10 shows, most gap quantification methods in the literature employed ablation gap characteristics (i.e., number, length and position of gaps) for evaluation. Similar to the evaluation of scars, these works also analyzed the correlation with EAM, by comparing the ablation gaps in LGE MRI to the electrical gaps in EAM. However, the applicability of EAM for ablation gap quantification is limited. This is mainly because: 1) the difficulty of the gap position registration between LGE MRI and EAM; 2) the voltage mapping does not entirely reflect scar/gap formation; 3) the requirement of a voltage threshold for scar/gap classification, with the same issues as for the LGE MRI threshold. Therefore, direct extrapolation of EAM data to verify LGE MRI should be performed carefully, in particular when they offer contradictory information (Nuñez-Garcia *et al.*, 2019). Besides, Ranjan *et al.* (2012) calculated the correlation between gap length (GL) measured via LGE MRI for evaluation. Nuñez-Garcia *et al.* (2019) proposed a quantitative index, i.e., relative gap measure (RGM), to calculate the proportion of the ablation gaps on a defined standard LA parcellation.

$$RGM = \frac{\text{Gap length}}{\text{Encircling Path length}}, \quad (17)$$

where “Gap length” indicates the sum of all GLs along the “Encircling Path”, and the “Encircling Path length” refers to the length of the complete closed loop on the PVs. The RGM is between 0 and 1, which means that if $RGM = 0$, the vein is completely surrounded, and if $RGM = 1$, there are no scars around the veins. To alleviate the effect of the scar segmentation, one could adopt a multi-threshold scheme for scar segmentation, and then integrate the results into the RGM calculation (Nuñez-Garcia *et al.*, 2019).

5. Potential clinical applications of the developed algorithms

It is essential to evaluate clinical utility of the developed approaches for AF. Besides, the exploration and understanding of potential clinical applications of AF can guide the development of segmentation and quantification algorithms, and answer important clinical questions. For example, we can employ the developed segmentation and quantification techniques to: 1) compare native and ablation-induced scars; 2) inspect the regional distribution of wall thickness, fibrosis/ scars and ablation gaps from LGE MRI; 3) analyze the relationship between fibrosis/ scars/ gaps and AF recurrence; 4) analyze the relationship between the low-voltage regions in EAM and scars detected by LGE MRI; 5) analyze the relationship between ablation parameters (power of the radiofrequency signal, catheter contact

force, etc.) and the created chronic lesion detected by LGE MRI; 6) assess the reproducibility of LGE MRI scar imaging with respect to imaging parameters. In this section, we mainly discuss the clinical applications 1-3, which only involve single-center LGE MRI data. In contrast, other three applications require additional EAM data or LGE MRIs with different ablation and imaging parameters.

5.1. Comparisons of native and ablation-induced scars

Recent studies demonstrated the differences in the extent and distribution of fibrosis/ scars of pre-/ post-ablation LGE MRI (Malcolme-Lawes *et al.*, 2013; Fukumoto *et al.*, 2015). For instance, Malcolme-Lawes *et al.* (2013) found that there was no difference of scars between ostial and LA cavity regions for pre-ablation data, but in post-ablation data the extent of scars in the ostia is larger than that in the LA cavity. They also reported a positive association between the extent of preexisting fibrosis and AF recurrence, which coincides with the finding in the literature (Verma *et al.*, 2005b; Mahnkopf *et al.*, 2010). However, they did not find any relationship between the amount of ablation-induced scars and AF recurrence, which should be negatively associated according to the studies of Peters *et al.* (2009); McGann *et al.* (2011). Fukumoto *et al.* (2015) demonstrated that ablation-induced scars are related to greater contrast affinity and thinner walls compared to preexisting fibrosis. Yang *et al.* (2017a) tried to distinguish native and ablation-induced scars via a texture based feature extraction. They stated the difficulty of the differentiation between native and ablation-induced scars, especially for longstanding persistent AF. Therefore, the understanding of the characteristics of pre- vs. post-ablation scars can be important and may inform future ablation strategies for AF.

5.2. Regional distribution analysis of wall thickness and fibrosis/ scars

To date, there are already several studies on LA wall thickness measurements, to analyze the relationships between wall thickness and patient age, AF stage/ type, scar formation, and AF recurrence (Karim *et al.*, 2018). For example, Hall *et al.* (2006) studied 34 patients with different ages and found that the thinnest and thickest area were roof (1.06 ± 1.49 mm) and septum (2.2 ± 0.82 mm), respectively. They did not find any significant relationships between the wall thickness and age. In contrast, Pan *et al.* (2008) measured the wall thickness on 180 AF patients with various ages and concluded that the thickness increased with age. They also found that the anterior wall (2.0 ± 0.9 mm, 3.2 ± 0.2 mm and 3.7 ± 0.9 mm in 40~60, 60~80 and 80+ year olds) was thicker than the posterior wall (0.7 ± 0.2 mm, 1.8 ± 0.2 mm and 2.4 ± 0.4 mm in 40~60, 60~80 and 80+ year olds) among all the age groups. Beinart *et al.* (2011) and Hayashi *et al.* (2014) both observed that the middle superior posterior wall was the thinnest region with a thickness of 1.43 ± 0.44 mm and 1.44 ± 0.17 mm, respectively. Suenari *et al.* (2013) analyzed the thickness on 54 AF patients, and showed that the thickest wall area is in the left lateral ridge (4.42 ± 1.28 mm), while the thinnest is in the LIPV (1.68 ± 0.27 mm). Besides, they found that the thickness of the left lateral ridge was

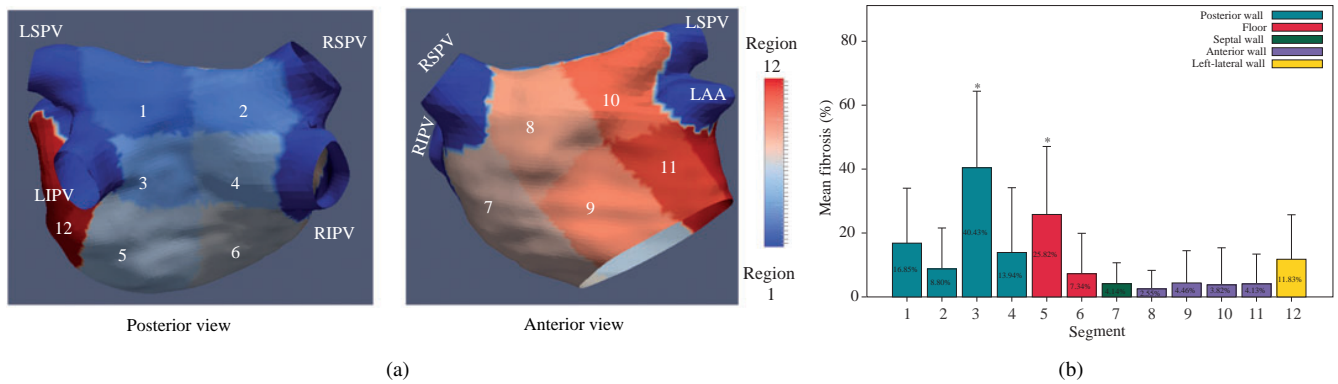


Fig. 7. Example of the LA parcellation and its corresponding fibrosis distribution: (a) the LA surface template parcellated from anatomical landmarks; (b) the regional distribution of LA fibrosis. Illustrations adopted from Benito et al. (2018).

correlated to the AF recurrence ($p=0.041$). However, the superior right posterior wall was found to be significantly associated with both AF recurrence ($p=0.048$) and electrical reconnection ($p=0.014$) in Inoue et al. (2016). Despite this progress, most of these works were based on manual segmented LA wall, and focused on CT image instead of LGE MRI. Note that transmural lesion formation is critical to the success of AF ablation and is dependent on regional LA wall thickness. Therefore, the distribution analysis of wall thickness from LGE MRI could be important and might provide insight into the progress of the AF.

As for the regional distribution of fibrosis/ scars in the LA LGE MRI, related information is limited and has not been comprehensively reported. Cochet et al. (2015) divided the LA into four segments and reported an irregular fibrosis anatomical distribution. However, they found that fibrosis generally occurred more often on the posterior LA wall than anterior one, particularly in the area adjacent to and below LIPV. Benito et al. (2018) manually defined the LA parcellation with 12 sub-regions: 1~4, posterior wall; 5~6, floor; 7, septal wall; 8~11, anterior wall; 12, lateral wall (see Fig. 7 (a)). They selected 76 consecutive AF patients for analysis and also observed that the fibrosis was preferentially located at the posterior wall and floor around the antrum of the LIPV, i.e., segments 3 and 5 (40.42% and 25.82% fibrosis), as Fig. 7 (b) shows. In contrast, segments 8 and 10 (2.54% and 3.82% fibrosis) in the anterior wall contained the fewest fibrosis. Similar with the increased wall thickness in Pan et al. (2008), they found that age (>60 years old) was also significantly correlated to increased fibrosis ($p=0.04$). Recently, (Lee et al., 2019) separated the LA into nine segments, and also found that scars were seen the most frequently at the posterior wall around the LIPV. Besides, they studied on 195 paroxysmal and 121 persistent AF patients, and observed that the presence of fibrosis assessed in LIPV from LGE MRI was associated with the chronicity of AF. These preliminary research suggests that the knowledge of preferential fibrosis/ scar position may open further perspectives in ablation strategies, patient selection, and AF recurrence prediction.

5.3. Relationship analysis between fibrosis/ scars/ gaps and AF recurrence

As mentioned in Section 5.1, both the extent of preexisting fibrosis and ablation-induced scars are correlated with AF recurrence, but with opposite effects. Specifically, AF recurrence is positively associated with the extent of preexisting scars, but negatively related to that of post-ablation scars. The characteristics of pre- vs post-ablation scars may explain the seemingly paradox and inform future strategies for ablation (Fukamoto et al., 2015). With respect to the pre-ablation scars (also namely fibrosis), it has been regarded as a potential cause of the abnormalities in atrial activation, which may underlie the initiation and maintenance of AF. Note that AF belongs to a progressive disease, and several studies revealed that causality between AF and fibrosis may be bidirectional (Oakes et al., 2009). This might explain why patients with a greater extent of fibrosis normally suffer much higher recurrence rates after ablation. Apart from the extent of fibrosis, Oakes et al. (2009) investigated 81 AF patients with pre-ablation LGE MRI, and found that AF recurrence also related to the locations of fibrosis. In their experiments, patients with recurrent AF presented fibrosis on the whole LA, whereas patients without recurrent AF had fibrosis only located primarily to the posterior wall and septum. As for post-ablation scars, robust evidence supports that complete circumferential and transmural lesion formation are critical to successful AF ablation (Cappato et al., 2003; Verma et al., 2005a; Ouyang et al., 2005). Here, the ablation lesion just refers to the post-ablation scars or can be named ablation-induced scars. Therefore, patients with smaller degree of post-ablation scars on LGE MRI tend to recur AF after ablation. Similar with fibrosis, the location of post-ablation scars is also an important index for AF recurrence prediction. For example, several studies emphasized the importance of right inferior PV (RIPV) scars, which is the most highly correlated to clinical ablation success (Yamada et al., 2006; Peters et al., 2009). This could attribute to the reported technical difficulty in ablating the RIPV region due to poor catheter access, resulting in its greater variability of scars. For example, Peters et al. (2009) studied on 35 AF patients undergoing the first ablation procedure, and compared the extent of scars on different sub-regions. They demonstrated that the PVs of patients without recurrence had more completely cir-

cumferential scars, especially on RIPV regions. In the case of ablation gaps, which are generally caused by incomplete PVI, the extend and distribution of gaps are regarded to be positively associated with AF recurrence. The identification and localization of ablation gaps from LGE MRI have been used to predict AF recurrence and further guide repeated PVI procedures (Bisbal *et al.*, 2014).

6. Discussion and future perspectives

6.1. Imaging quality analysis of LGE MRI

LGE MRI has attracted increasingly more attention for assessing AF before and after an ablation procedure. Automatic segmentation and quantification algorithms of LA tissues can facilitate the diagnosis and therapy of AF patients. However, LGE imaging is still challenging in comparison to other imaging techniques, due to the existence of contrast enhancement, its complex patterns, and the large quality and contrast variations across different patients. Especially, LGE MRI of LA wall requires substantially higher spatial resolution, patient-specific optimization of scan parameters, strict criteria for contrast dosage and delay between contrast injection and image acquisition, compared to LGE MRI of the left ventricle (Siebermair *et al.*, 2017; Chubb *et al.*, 2018). These precise requirements are difficult to meet in practice, resulting in poor image quality of LGE MRI.

Xiong *et al.* (2020); Karim *et al.* (2018, 2013) investigated the influence of image quality on the algorithm performance for LA, LA wall (from CT and non-enhanced MRI), and LA scar segmentation, respectively. To our knowledge, no study has been reported to analyzed the effect of LGE MRI quality on the accuracy of ablation gap quantification. In general, the images with better quality tend to yield higher accuracy, but there is no significant improvement reported in Karim *et al.* (2013). This could be attributed to the accurate initialization and possible minor range of image quality difference. Threshold methods, which are commonly used and are based on the intensity of blood pool regions for normalization (such as IIR), strongly depend on the image quality (Andalò *et al.*, 2018). Further research is desired to construct models that could extract useful features less dependent from the image quality, besides the advances in imaging acquisition,

6.2. Reproducibility analysis and model generalization

Despite the promising results from a few centers, the quantification of LA scars has not yet been widely adopted in clinical routine due to the poor reproducibility of LGE MRI (Benito *et al.*, 2017). This is mainly due to the absence of standardized LGE MRI acquisition protocols. Currently, most existing algorithms have only been evaluated on center- and vendor-specific LGE MRI. Though the *Left Atrium Fibrosis and Scar Segmentation Challenge* offered multi-center and multi-scanner data, the benchmark algorithms only tested on center- and vendor-specific images. It was not clear about their suitability and performance in data from other centers or vendors (Karim *et al.*, 2013). Note that the LGE MRIs from different centers can vary evidently in appearance, as Fig. 8 shows. Even in the same

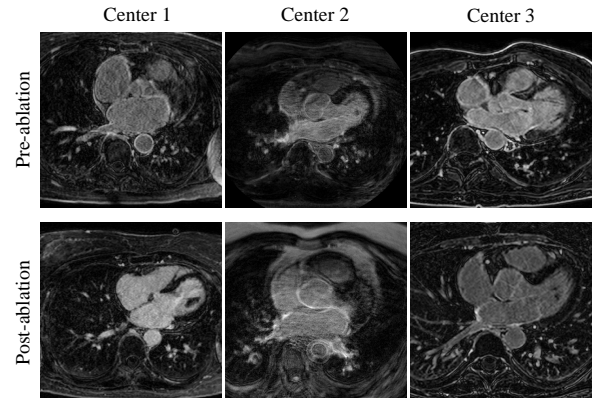


Fig. 8. Multi-center pre- and post-ablation LGE MRIs. The images differ in contrast, enhancement and background.

dataset, one could encounter a severe data mismatch problem, resulting in poor outlier results Li *et al.* (2020c). Therefore, large multi-center and multi-scanner datasets are needed, to validate the robustness and generalizability of proposed methods. It is also worthy of promoting deep models with efficient inherent generalization abilities for LGE MRI data processing from different centers and vendors.

6.3. Joint optimization and independence analysis

The target regions of the four tasks reviewed in Section 3 are all inherently related, particularly in the spatial information of images, as shown in Fig. 2. Several studies employed multi-task learning for simultaneous LA segmentation and scar segmentation/ quantification, and proved the effectiveness of joint optimization (Chen *et al.*, 2018b; Li *et al.*, 2020a). The spatial information between LA and scars could simply be learned via spatial attention, i.e., multiplying the LA blood pool feature map by the scar feature map (Chen *et al.*, 2018b), or projecting the scars onto the LA endocardial surface (Li *et al.*, 2020a). However, neither of the two schemes considered the information of the LA wall, where the scars are located. Note that joint optimization schemes could also alleviate the class-imbalance problem existing in the segmentation and quantification of small regions, such as scars and ablation gaps. Nevertheless, more exploration of effective joint optimization on related tasks of AF is required, especially between LA wall and scar segmentation.

It can be interesting and crucial to study, and then mitigate the effect of inaccurate LA/ LA wall segmentation on the following scar/ gap segmentation and quantification. Li *et al.* (2020b) developed a patch shift scheme for scar quantification to reduce the dependence on accurate LA segmentation, but the tasks were not simultaneously optimized. Li *et al.* (2020a) learned the spatial information scar and normal wall regions via distance probability maps, and compared these two probabilities instead of employing a fixed threshold to extract scars. By comparing the two probabilities, more stable than only using the probability of scars, they mitigated the effect of inaccurate LA segmentation. Despite these studies, the joint optimization and independence analysis of the AF-related tasks are yet to be explored in more depth in the future.

7. Conclusion

We have presented and discussed current progress of LGE MRI computing for LA studies, particularly for the four tasks, including segmentation and (or) quantification of LA cavity, wall, scars and ablation gaps. Though LGE MRI has been proven to be a powerful diagnostic and prognostic tool in the study of AF, a standardized imaging protocol should be further investigated. Furthermore, limited number of works have been reported focusing on image computing tasks, especially for automatic LA wall segmentation and ablation gap quantification. Most research relies on manual delineation for further analysis and clinical applications. Therefore, more accurate and robust automatic methods are desired for overall wide and intelligent use in the clinical setting. The data-driven approaches have shown great potential for the LA and LA scar segmentation and quantification, thanks to the development of deep neural networks. The joint optimization of these related tasks can be a new direction for the utilization of their spatial relationship. To research for a broader clinical application, well-controlled and large-cohorted studies are expected to better guarantee the reproducibility of measurements, refine the evaluation methods, and validate the impact on clinical outcomes as well as the computing accuracy.

Acknowledgment

This work was supported by the National Natural Science Foundation of China (61971142, 62111530195 and 62011540404) and the development fund for Shanghai talents (2020015). L Li was partially supported by the CSC Scholarship. JA Schnabel and VA Zimmer would like to acknowledge funding from a Wellcome Trust IEH Award (WT 102431), an EPSRC programme grant (EP/P001009/1), and the Wellcome/EPSRC Center for Medical Engineering (WT 203148/Z/16/Z).

References

Akoum, N., Daccarett, M., McGann, C., Segerson, N., Vergara, G., Kuppahally, S., Badger, T., Burgon, N., Haslam, T., Kholmovski, E., et al., 2011. Atrial fibrosis helps select the appropriate patient and strategy in catheter ablation of atrial fibrillation: A DE-MRI guided approach. *Journal of Cardiovascular Electrophysiology* 22, 16–22.

Akoum, N., Wilber, D., Hindricks, G., Jais, P., Cates, J., Marchlinski, F., Kholmovski, E., Burgon, N., Hu, N., Mont, L., et al., 2015. MRI assessment of ablation-induced scarring in atrial fibrillation: analysis from the DECAAF study. *Journal of Cardiovascular Electrophysiology* 26, 473–480.

Andalò, A., Fabbri, C., Valinoti, M., Masci, A., Corsi, C., 2018. Quantification of left atrium fibrosis from LGE MRI in atrial fibrillation, in: 2018 Computing in Cardiology Conference (CinC), IEEE. pp. 1–4.

Arujuna, A., Karim, R., Caulfield, D., Knowles, B., Rhode, K., Schaeffer, T., Kato, B., Rinaldi, C.A., Cooklin, M., Razavi, R., et al., 2012. Acute pulmonary vein isolation is achieved by a combination of reversible and irreversible atrial injury after catheter ablation: evidence from magnetic resonance imaging. *Circulation: Arrhythmia and Electrophysiology* 5, 691–700.

Badger, T.J., Daccarett, M., Akoum, N.W., Adjei-Poku, Y.A., Burgon, N.S., Haslam, T.S., Kalvaitis, S., Kuppahally, S., Vergara, G., McMullen, L., et al., 2010. Evaluation of left atrial lesions after initial and repeat atrial fibrillation ablation: lessons learned from delayed-enhancement MRI in repeat ablation procedures. *Circulation: Arrhythmia and Electrophysiology* 3, 249–259.

Bakalli, A., Koçınaj, D., Georgievska-Ismail, L., Bekteshi, T., Pillana, E., Sejdiu, B., 2012. Right bundle branch block as a marker for interatrial septal abnormalities. *Cardiology in the Young* 22, 18.

Beinart, R., Abbata, S., Blum, A., Ferencik, M., Heist, K., Ruskin, J., Mansour, M., 2011. Left atrial wall thickness variability measured by CT scans in patients undergoing pulmonary vein isolation. *Journal of Cardiovascular Electrophysiology* 22, 1232–1236.

Benito, E.M., Cabanelas, N., Nuñez-García, M., Alarcón, F., Figueras I Ventura, R.M., Soto-Iglesias, D., Guasch, E., Prat-Gonzalez, S., Perea, R.J., Borràs, R., et al., 2018. Preferential regional distribution of atrial fibrosis in posterior wall around left inferior pulmonary vein as identified by late gadolinium enhancement cardiac magnetic resonance in patients with atrial fibrillation. *Ep Europace* 20, 1959–1965.

Benito, E.M., Carlosena-Remirez, A., Guasch, E., Prat-González, S., Perea, R.J., Figueras, R., Borràs, R., Andreu, D., Arbelo, E., Tolosana, J.M., et al., 2017. Left atrial fibrosis quantification by late gadolinium-enhanced magnetic resonance: a new method to standardize the thresholds for reproducibility. *Ep Europace* 19, 1272–1279.

Berrueto, A., Tamborero, D., Mont, L., Benito, B., Tolosana, J.M., Sitges, M., Vidal, B., Arriagada, G., Méndez, F., Mattiello, M., et al., 2007. Pre-procedural predictors of atrial fibrillation recurrence after circumferential pulmonary vein ablation. *European Heart Journal* 28, 836–841.

Bian, C., Yang, X., Ma, J., Zheng, S., Liu, Y.A., Nezafat, R., Heng, P.A., Zheng, Y., 2018. Pyramid network with online hard example mining for accurate left atrium segmentation, in: International Workshop on Statistical Atlases and Computational Models of the Heart, Springer. pp. 237–245.

Bisbal, F., Guiu, E., Cabanas-Grandío, P., Berrueto, A., Prat-Gonzalez, S., Vidal, B., Garrido, C., Andreu, D., Fernandez-Armenta, J., Tolosana, J.M., et al., 2014. Cmr-guided approach to localize and ablate gaps in repeat AF ablation procedure. *JACC: Cardiovascular Imaging* 7, 653–663.

Bishop, M., Rajani, R., Plank, G., Gaddum, N., Carr-White, G., Wright, M., O'Neill, M., Niederer, S., 2016. Three-dimensional atrial wall thickness maps to inform catheter ablation procedures for atrial fibrillation. *Europace* 18, 376–383.

Borra, D., Andalò, A., Paci, M., Fabbri, C., Corsi, C., 2020. A fully automated left atrium segmentation approach from late gadolinium enhanced magnetic resonance imaging based on a convolutional neural network. *Quantitative Imaging in Medicine and Surgery* 10, 1894.

Borra, D., Masci, A., Esposito, L., Andalò, A., Fabbri, C., Corsi, C., 2018. A semantic-wise convolutional neural network approach for 3-D left atrium segmentation from late gadolinium enhanced magnetic resonance imaging, in: International Workshop on Statistical Atlases and Computational Models of the Heart, Springer. pp. 329–338.

Calkins, H., Brugada, J., Packer, D.L., Cappato, R., Chen, S.A., Crijns, H.J., Damiano Jr, R.J., Davies, D.W., Haines, D.E., Haissaguerre, M., et al., 2007. Hrs/ehra/ecas expert consensus statement on catheter and surgical ablation of atrial fibrillation: Recommendations for personnel, policy, procedures and follow-up: A report of the heart rhythm society (HRS) task force on catheter and surgical ablation of atrial fibrillation developed in partnership with the european heart rhythm association (EHRA) and the european cardiac arrhythmia society (ECAS); in collaboration with the american college of cardiology (ACC), american heart association (AHA), and the society of thoracic surgeons (STS). endorsed and approved by the governing bodies of the american college of cardiology, the american heart association, the european cardiac arrhythmia society, the european heart rhythm association, the society of thoracic surgeons, and the heart rhythm society. *Europace* 9, 335–379.

Cappato, R., Negroni, S., Pecora, D., Bentivegna, S., Lupo, P.P., Carolei, A., Esposito, C., Furlanello, F., De Ambroggi, L., 2003. Prospective assessment of late conduction recurrence across radiofrequency lesions producing electrical disconnection at the pulmonary vein ostium in patients with atrial fibrillation. *Circulation* 108, 1599–1604.

Casaclang-Verzosa, G., Gersh, B.J., Tsang, T.S., 2008. Structural and functional remodeling of the left atrium: clinical and therapeutic implications for atrial fibrillation. *Journal of the American College of Cardiology* 51, 1–11.

Chen, C., Bai, W., Rueckert, D., 2018a. Multi-task learning for left atrial segmentation on GE-MRI, in: International Workshop on Statistical Atlases and Computational Models of the Heart, Springer. pp. 292–301.

Chen, C., Qin, C., Qiu, H., Tarroni, G., Duan, J., Bai, W., Rueckert, D., 2020. Deep learning for cardiac image segmentation: A review. *Frontiers in Cardiovascular Medicine* 7, 25.

- Chen, J., Yang, G., Gao, Z., Ni, H., Angelini, E., Mohiaddin, R., Wong, T., Zhang, Y., Du, X., Zhang, H., et al., 2018b. Multiview two-task recursive attention model for left atrium and atrial scars segmentation, in: International Conference on Medical Image Computing and Computer-Assisted Intervention, Springer. pp. 455–463.
- Chubb, H., Karim, R., Roujol, S., Nuñez-García, M., Williams, S.E., Whitaker, J., Harrison, J., Butakoff, C., Camara, O., Chiribiri, A., et al., 2018. The reproducibility of late gadolinium enhancement cardiovascular magnetic resonance imaging of post-ablation atrial scar: a cross-over study. *Journal of Cardiovascular Magnetic Resonance* 20, 21.
- Chugh, S.S., Havmoeller, R., Narayanan, K., Singh, D., Rienstra, M., Benjamin, E.J., Gillum, R.F., Kim, Y.H., McAnulty Jr, J.H., Zheng, Z.J., et al., 2014. Worldwide epidemiology of atrial fibrillation: a global burden of disease 2010 study. *Circulation* 129, 837–847.
- Cochet, H., Mouries, A., Nivet, H., Sacher, F., Derval, N., Denis, A., Merle, M., Relan, J., Hocini, M., Haissaguerre, M., et al., 2015. Age, atrial fibrillation, and structural heart disease are the main determinants of left atrial fibrosis detected by delayed-enhanced magnetic resonance imaging in a general cardiology population. *Journal of Cardiovascular Electrophysiology* 26, 484–492.
- Cox, J.L., 2003. Surgical treatment of atrial fibrillation: a review. *EP Europace* 5, S20–S29.
- Deng, C., Zhang, X., 2016. Automatic segmentation of the left atrium from mr images via semantic information, in: 2016 IEEE International Conference on Systems, Man, and Cybernetics (SMC), IEEE. pp. 003312–003316.
- Du, X., Yin, S., Tang, R., Liu, Y., Song, Y., Zhang, Y., Liu, H., Li, S., 2020. Segmentation and visualization of left atrium through a unified deep learning framework. *International Journal of Computer Assisted Radiology and Surgery*, 1–12.
- Dzeshka, M.S., Lip, G.Y., Snezhitskiy, V., Shantsila, E., 2015. Cardiac fibrosis in patients with atrial fibrillation: mechanisms and clinical implications. *Journal of the American College of Cardiology* 66, 943–959.
- Fukumoto, K., Habibi, M., Ipek, E.G., Khurram, I.M., Zimmerman, S.L., Zipunnikov, V., Spragg, D.D., Ashikaga, H., Rickard, J., Marine, J.E., et al., 2015. Comparison of preexisting and ablation-induced late gadolinium enhancement on left atrial magnetic resonance imaging. *Heart Rhythm* 12, 668–672.
- Galand, V., Pavin, D., Behar, N., Auffret, V., Fénéon, D., Behaghel, A., Daubert, J.C., Mabo, P., Martins, R.P., 2016. Localization of gaps during redo ablations of paroxysmal atrial fibrillation: preferential patterns depending on the choice of cryoballoon ablation or radiofrequency ablation for the initial procedure. *Archives of Cardiovascular Diseases* 109, 591–598.
- Gao, Y., Gholami, B., MacLeod, R.S., Blauer, J., Haddad, W.M., Tannenbaum, A.R., 2010. Segmentation of the endocardial wall of the left atrium using local region-based active contours and statistical shape learning, in: Medical Imaging 2010: Image Processing, International Society for Optics and Photonics. p. 76234Z.
- Gottlieb, I., Pinheiro, A., Brinker, J.A., Corretti, M.C., Mayer, S.A., Bluemke, D.A., Lima, J.A., Marine, J.E., Berger, R.D., Calkins, H., et al., 2008. Diagnostic accuracy of arterial phase 64-slice multidetector CT angiography for left atrial appendage thrombus in patients undergoing atrial fibrillation ablation. *Journal of Cardiovascular Electrophysiology* 19, 247–251.
- Habijan, M., Babin, D., Galić, I., Leventić, H., Romić, K., Velicki, L., Pižurica, A., 2020. Overview of the whole heart and heart chamber segmentation methods. *Cardiovascular Engineering and Technology*, 1–23.
- Hall, B., Jeevanantham, V., Simon, R., Filippone, J., Vorobiof, G., Daubert, J., 2006. Variation in left atrial transmural wall thickness at sites commonly targeted for ablation of atrial fibrillation. *Journal of Interventional Cardiac Electrophysiology* 17, 127–132.
- Harrison, J.L., Jensen, H.K., Peel, S.A., Chiribiri, A., Grøndal, A.K., Bloch, L.Ø., Pedersen, S.F., Bentzon, J.F., Kolbitsch, C., Karim, R., et al., 2014. Cardiac magnetic resonance and electroanatomical mapping of acute and chronic atrial ablation injury: a histological validation study. *European Heart Journal* 35, 1486–1495.
- Harrison, J.L., Sohns, C., Linton, N.W., Karim, R., Williams, S.E., Rhode, K.S., Gill, J., Cooklin, M., Rinaldi, C.A., Wright, M., et al., 2015a. Repeat left atrial catheter ablation: cardiac magnetic resonance prediction of endocardial voltage and gaps in ablation lesion sets. *Circulation: Arrhythmia and Electrophysiology* 8, 270–278.
- Harrison, J.L., Whitaker, J., Chubb, H., Williams, S.E., Wright, M., Razavi, R.S., O'Neill, M.D., 2015b. Advances in CMR of post-ablation atrial injury. *Current Cardiovascular Imaging Reports* 8, 22.
- Hayashi, H., Hayashi, M., Miyauchi, Y., Takahashi, K., Uetake, S., Tsuboi, I., Yodogawa, K., Iwasaki, Y.K., Shimizu, W., 2014. Left atrial wall thickness and outcomes of catheter ablation for atrial fibrillation in patients with hypertrophic cardiomyopathy. *Journal of Interventional Cardiac Electrophysiology* 40, 153–160.
- Higuchi, K., Cates, J., Gardner, G., Morris, A., Burgon, N.S., Akoum, N., Marrouche, N.F., 2018. The spatial distribution of late gadolinium enhancement of left atrial magnetic resonance imaging in patients with atrial fibrillation. *JACC: Clinical Electrophysiology* 4, 49–58.
- Holmes, D.R., Monahan, K.H., Packer, D., 2009. Pulmonary vein stenosis complicating ablation for atrial fibrillation: clinical spectrum and interventional considerations. *JACC: Cardiovascular Interventions* 2, 267–276.
- Hsing, J., Peters, D.C., Knowles, B.R., Manning, W.J., Josephson, M.E., 2014. Cardiovascular magnetic resonance imaging of scar development following pulmonary vein isolation: a prospective study. *PLoS one* 9, e104844.
- Hunter, R.J., Jones, D.A., Boubertakh, R., MALCOLME-LAWES, L.C., Kanagaratnam, P., Juli, C.F., Davies, D.W., Peters, N.S., Baker, V., Earley, M.J., et al., 2013. Diagnostic accuracy of cardiac magnetic resonance imaging in the detection and characterization of left atrial catheter ablation lesions: a multicenter experience. *Journal of Cardiovascular Electrophysiology* 24, 396–403.
- Inoue, J., Drangova, M., 2016. Left atrial wall segmentation using clinically correlated metrics, in: International Workshop on Statistical Atlases and Computational Models of the Heart, Springer. pp. 201–210.
- Inoue, J., Skanes, A.C., Gula, L.J., Drangova, M., 2016. Effect of left atrial wall thickness on radiofrequency ablation success. *Journal of Cardiovascular Electrophysiology* 27, 1298–1303.
- Inoue, J., Skanes, A.C., White, J.A., Rajchl, M., Drangova, M., 2014. Patient-specific left atrial wall-thickness measurement and visualization for radiofrequency ablation, in: Medical Imaging 2014: Image-Guided Procedures, Robotic Interventions, and Modeling, International Society for Optics and Photonics. p. 90361N.
- Jamart, K., Xiong, Z., Talou, G.D.M., Stiles, M.K., Zhao, J., 2020. Mini review: Deep learning for atrial segmentation from late gadolinium-enhanced MRIs. *Frontiers in Cardiovascular Medicine* 7.
- Jamart, K., Xiong, Z., Talou, G.M., Stiles, M.K., Zhao, J., 2019. Two-stage 2D CNN for automatic atrial segmentation from LGE-MRIs, in: International Workshop on Statistical Atlases and Computational Models of the Heart, Springer. pp. 81–89.
- Jannin, P., Krupinski, E., Warfield, S.K., 2006. Validation in medical image processing. *IEEE Transactions on Medical Imaging* 25, 1405–9.
- Jia, S., Cadour, L., Cochet, H., Sermesant, M., 2016. Stacom-slant challenge: left atrial wall segmentation and thickness measurement using region growing and marker-controlled geodesic active contour, in: International Workshop on Statistical Atlases and Computational Models of the Heart, Springer. pp. 211–219.
- Jia, S., Despinasse, A., Wang, Z., Delingette, H., Pennec, X., Jaïs, P., Cochet, H., Sermesant, M., 2018. Automatically segmenting the left atrium from cardiac images using successive 3D U-nets and a contour loss, in: International Workshop on Statistical Atlases and Computational Models of the Heart, Springer. pp. 221–229.
- Jongbloed, M., Schali, M., Zeppenfeld, K., Oemrawsingh, P., van der Wall, E., Bax, J., 2005. Clinical applications of intracardiac echocardiography in interventional procedures. *Heart* 91, 981–990.
- Karim, R., Arujuna, A., Brazier, A., Gill, J., Rinaldi, C.A., O'Neill, M., Razavi, R., Schaeffer, T., Rueckert, D., Rhode, K.S., 2011. Automatic segmentation of left atrial scar from delayed-enhancement magnetic resonance imaging, in: International Conference on Functional Imaging and Modeling of the Heart, Springer. pp. 63–70.
- Karim, R., Arujuna, A., Housden, R.J., Gill, J., Cliffe, H., Matharu, K., Gill, J., Rindaldi, C.A., O'Neill, M., Rueckert, D., et al., 2014. A method to standardize quantification of left atrial scar from delayed-enhancement MR images. *IEEE Journal of Translational Engineering in Health and Medicine* 2, 1–15.
- Karim, R., Blake, L.E., Inoue, J., Tao, Q., Jia, S., Housden, R.J., Bhagirath, P., Duval, J.L., Varela, M., Behar, J.M., et al., 2018. Algorithms for left atrial wall segmentation and thickness—evaluation on an open-source CT and MRI image database. *Medical Image Analysis* 50, 36–53.
- Karim, R., Housden, R.J., Balasubramaniam, M., Chen, Z., Perry, D., Uddin, A., Al-Beyati, Y., Palkhi, E., Acheampong, P., Obom, S., et al., 2013. Evaluation of current algorithms for segmentation of scar tissue from late gadolinium enhancement cardiovascular magnetic resonance of the left

- atrium: an open-access grand challenge. *Journal of Cardiovascular Magnetic Resonance* 15, 105.
- Karim, R., Juli, C., Malcolm-Lawes, L., Wyn-Davies, D., Kanagaratnam, P., Peters, N., Rueckert, D., 2010. Automatic segmentation of left atrial geometry from contrast-enhanced magnetic resonance images using a probabilistic atlas, in: *International Workshop on Statistical Atlases and Computational Models of the Heart*, Springer. pp. 134–143.
- Karim, R., Rhode, K., 2016. Left atrial wall thickness challenge (SLAWT). https://www.doc.ic.ac.uk/~rkarim/la_lv_framework/wall/index.html.
- Knowles, B.R., Caulfield, D., Cooklin, M., Rinaldi, C.A., Gill, J., Bostock, J., Razavi, R., Schaeffter, T., Rhode, K.S., 2010. 3-D visualization of acute rf ablation lesions using MRI for the simultaneous determination of the patterns of necrosis and edema. *IEEE Transactions on Biomedical Engineering* 57, 1467–1475.
- Kutra, D., Saalbach, A., Lehmann, H., Groth, A., Dries, S.P., Krueger, M.W., Dössel, O., Weese, J., 2012. Automatic multi-model-based segmentation of the left atrium in cardiac MRI scans, in: *International Conference on Medical Image Computing and Computer-Assisted Intervention*, Springer. pp. 1–8.
- Lee, D.K., Shim, J., Choi, J.I., Kim, Y.H., Oh, Y.W., Hwang, S.H., 2019. Left atrial fibrosis assessed with cardiac MRI in patients with paroxysmal and those with persistent atrial fibrillation. *Radiology* 292, 575–582.
- Li, C., Tong, Q., Liao, X., Si, W., Sun, Y., Wang, Q., Heng, P.A., 2018a. Attention based hierarchical aggregation network for 3D left atrial segmentation, in: *International Workshop on Statistical Atlases and Computational Models of the Heart*, Springer. pp. 255–264.
- Li, L., Weng, X., Schnabel, J.A., Zhuang, X., 2020a. Joint left atrial segmentation and scar quantification based on a DNN with spatial encoding and shape attention, in: *International Conference on Medical Image Computing and Computer-Assisted Intervention*, Springer. pp. 118–127.
- Li, L., Wu, F., Yang, G., Xu, L., Wong, T., Mohiaddin, R., Firmin, D., Keegan, J., Zhuang, X., 2020b. Atrial scar quantification via multi-scale CNN in the graph-cuts framework. *Medical Image Analysis* 60, 101595.
- Li, L., Yang, G., Wu, F., Wong, T., Mohiaddin, R., Firmin, D., Keegan, J., Xu, L., Zhuang, X., 2018b. Atrial scar segmentation via potential learning in the graph-cut framework, in: *International Workshop on Statistical Atlases and Computational Models of the Heart*, Springer. pp. 152–160.
- Li, L., Zimmer, V.A., Ding, W., Wu, F., Huang, L., Schnabel, J.A., Zhuang, X., 2021. Random style transfer based domain generalization networks integrating shape and spatial information, in: *International Workshop on Statistical Atlases and Computational Models of the Heart*, Springer. pp. 208–218.
- Li, L., Zimmer, V.A., Schnabel, J.A., Zhuang, X., 2020c. AtrialJSQnet: A new framework for joint segmentation and quantification of left atrium and scars incorporating spatial and shape information. *arXiv preprint arXiv:2008.04729*.
- Linhart, M., Alarcon, F., Borrás, R., Benito, E.M., Chirpa, F., Cozzari, J., Caixal, G., Enomoto, N., Carlosena, A., Guasch, E., et al., 2018. Delayed gadolinium enhancement magnetic resonance imaging detected anatomic gap length in wide circumferential pulmonary vein ablation lesions is associated with recurrence of atrial fibrillation. *Circulation: Arrhythmia and Electrophysiology* 11, e006659.
- Liu, Y., Dai, Y., Yan, C., Wang, K., 2018. Deep learning based method for left atrial segmentation in GE-MRI, in: *International Workshop on Statistical Atlases and Computational Models of the Heart*, Springer. pp. 311–318.
- Mahnkopf, C., Badger, T.J., Burgon, N.S., Dacarett, M., Haslam, T.S., Badger, C.T., McGann, C.J., Akoum, N., Kholmovski, E., Macleod, R.S., et al., 2010. Evaluation of the left atrial substrate in patients with lone atrial fibrillation using delayed-enhanced MRI: implications for disease progression and response to catheter ablation. *Heart Rhythm* 7, 1475–1481.
- Malcolm-Lawes, L., Juli, C., Karim, R., Bai, W., Quest, R., Lim, P.B., Jamil-Copley, S., Kojodjojo, P., Ariff, B., Davies, D., et al., 2013. Automated analysis of atrial late gadolinium enhancement imaging that correlates with endocardial voltage and clinical outcomes: a 2-center study. *Heart Rhythm* 10, 1184–1191.
- Marrouche, N.F., Wilber, D., Hindricks, G., Jais, P., Akoum, N., Marchlinski, F., Kholmovski, E., Burgon, N., Hu, N., Mont, L., et al., 2014. Association of atrial tissue fibrosis identified by delayed enhancement MRI and atrial fibrillation catheter ablation: the DECAAF study. *Jama* 311, 498–506.
- McGann, C., Akoum, N., Patel, A., Kholmovski, E., Revelo, P., Damal, K., Wilson, B., Cates, J., Harrison, A., Ranjan, R., et al., 2014. Atrial fibrillation ablation outcome is predicted by left atrial remodeling on MRI. *Circulation: Arrhythmia and Electrophysiology* 7, 23–30.
- McGann, C., Kholmovski, E., Blauer, J., Vijayakumar, S., Haslam, T., Cates, J., DiBella, E., Burgon, N., Wilson, B., Alexander, A., et al., 2011. Dark regions of no-reflow on late gadolinium enhancement magnetic resonance imaging result in scar formation after atrial fibrillation ablation. *Journal of the American College of Cardiology* 58, 177–185.
- Miller, M.A., d'Avila, A., Dukkipati, S.R., Koruth, J.S., Viles-Gonzalez, J., Napolitano, C., Eggert, C., Fischer, A., Gomes, J.A., Reddy, V.Y., 2012. Acute electrical isolation is a necessary but insufficient endpoint for achieving durable PV isolation: the importance of closing the visual gap. *Europace* 14, 653–660.
- Mishima, T., Miyamoto, K., Morita, Y., Kamakura, T., Nakajima, K., Yamagata, K., Wada, M., Ishibashi, K., Inoue, Y., Nagase, S., et al., 2019. Feasibility of late gadolinium enhancement magnetic resonance imaging to detect ablation lesion gaps in patients undergoing cryoballoon ablation of paroxysmal atrial fibrillation. *Journal of Arrhythmia* 35, 190–196.
- Mohrs, O.K., Nowak, B., Petersen, S.E., Welsner, M., Rubel, C., Magedanz, A., Kauczor, H.U., Voigtlaender, T., 2006. Thrombus detection in the left atrial appendage using contrast-enhanced MRI: a pilot study. *American Journal of Roentgenology* 186, 198–205.
- Nattel, S., 2002. New ideas about atrial fibrillation 50 years on. *Nature* 415, 219–226.
- Njoku, A., Kannabhiran, M., Arora, R., Reddy, P., Gopinathannair, R., Lakkireddy, D., Dominic, P., 2018. Left atrial volume predicts atrial fibrillation recurrence after radiofrequency ablation: a meta-analysis. *Ep Europace* 20, 33–42.
- Núñez-García, M., Camara, O., O'Neill, M.D., Razavi, R., Chubb, H., Butakoff, C., 2019. Mind the gap: quantification of incomplete ablation patterns after pulmonary vein isolation using minimum path search. *Medical Image Analysis* 51, 1–12.
- Núñez-García, M., Zhuang, X., Sanroma, G., Li, L., Xu, L., Butakoff, C., Camara, O., 2018. Left atrial segmentation combining multi-atlas whole heart labeling and shape-based atlas selection, in: *International Workshop on Statistical Atlases and Computational Models of the Heart*, Springer. pp. 302–310.
- Núñez García, M., et al., 2018. Left atrial parameterisation and multi-modal data analysis: application to atrial fibrillation. Ph.D. thesis. Universitat Pompeu Fabra.
- Oakes, R.S., Badger, T.J., Kholmovski, E.G., Akoum, N., Burgon, N.S., Fish, E.N., Blauer, J.J., Rao, S.N., DiBella, E.V., Segerson, N.M., et al., 2009. Detection and quantification of left atrial structural remodeling using delayed enhancement MRI in patients with atrial fibrillation. *Circulation* 119, 1758.
- Obeng-Gyimah, E., Nazarian, S., 2020. Advancements in imaging for atrial fibrillation ablation: Is there a potential to improve procedural outcomes? *The Journal of Innovations in Cardiac Rhythm Management* 11, 4172.
- Ouyang, F., Antz, M., Ernst, S., Hachiya, H., Mavrakis, H., Deger, F.T., Schauermann, A., Chun, J., Falk, P., Hennig, D., et al., 2005. Recovered pulmonary vein conduction as a dominant factor for recurrent atrial tachyarrhythmias after complete circular isolation of the pulmonary veins: lessons from double lasso technique. *Circulation* 111, 127–135.
- Pan, N.H., Tsao, H.M., Chang, N.C., Chen, Y.J., Chen, S.A., 2008. Aging dilates atrium and pulmonary veins: implications for the genesis of atrial fibrillation. *Chest* 133, 190–196.
- Peng, P., Lekadir, K., Gooya, A., Shao, L., Petersen, S.E., Frangi, A.F., 2016. A review of heart chamber segmentation for structural and functional analysis using cardiac magnetic resonance imaging. *Magnetic Resonance Materials in Physics, Biology and Medicine* 29, 155–195.
- Perry, D., Morris, A., Burgon, N., McGann, C., Macleod, R., Cates, J., 2012. Automatic classification of scar tissue in late gadolinium enhancement cardiac MRI for the assessment of left-atrial wall injury after radiofrequency ablation, in: *Medical Imaging 2012: Computer-Aided Diagnosis*, International Society for Optics and Photonics. p. 83151D.
- Peters, D.C., Wylie, J.V., Hauser, T.H., Nezafat, R., Han, Y., Woo, J.J., Tlacas, J., Kissinger, K.V., Goddu, B., Josephson, M.E., et al., 2009. Recurrence of atrial fibrillation correlates with the extent of post-procedural late gadolinium enhancement: a pilot study. *JACC: Cardiovascular Imaging* 2, 308–316.
- Polaczek, M., Szaro, P., Baranska, I., Burakowska, B., Ciszek, B., 2019. Morphology and morphometry of pulmonary veins and the left atrium in multislice computed tomography. *Surgical and Radiologic Anatomy* 41, 721–730.
- Pontecorvoli, G., Figueras i Ventura, R.M., Carlosena, A., Benito, E., Prat-Gonzales, S., Padeletti, L., Mont, L., 2017. Use of delayed-enhancement magnetic resonance imaging for fibrosis detection in the atria: a review. *EP*

- Europace 19, 180–189.
- Prasanna, L., Praveena, R., AS, D., Kumar, M., 2014. Variations in the pulmonary venous ostium in the left atrium and its clinical importance. *Journal of Clinical and Diagnostic Research: JCDR* 8, 10.
- Preetha, C.J., Haridasan, S., Abdi, V., Engelhardt, S., 2018. Segmentation of the left atrium from 3D gadolinium-enhanced mr images with convolutional neural networks, in: *International Workshop on Statistical Atlases and Computational Models of the Heart*, Springer. pp. 265–272.
- Puybureau, É., Zhao, Z., Khoudli, Y., Carlinet, E., Xu, Y., Lacotte, J., Géraud, T., 2018. Left atrial segmentation in a few seconds using fully convolutional network and transfer learning, in: *International Workshop on Statistical Atlases and Computational Models of the Heart*, Springer. pp. 339–347.
- Qiao, M., Wang, Y., van der Geest, R.J., Tao, Q., 2018. Fully automated left atrium cavity segmentation from 3D GE-MRI by multi-atlas selection and registration, in: *International Workshop on Statistical Atlases and Computational Models of the Heart*, Springer. pp. 230–236.
- Ranjan, R., Kato, R., Zviman, M.M., Dickfeld, T.M., Roguin, A., Berger, R.D., Tomaselli, G.F., Halperin, H.R., 2011. Gaps in the ablation line as a potential cause of recovery from electrical isolation and their visualization using MRI. *Circulation: Arrhythmia and Electrophysiology* 4, 279–286.
- Ranjan, R., Kholmovski, E.G., Blauer, J., Vijayakumar, S., Volland, N.A., Salama, M.E., Parker, D.L., MacLeod, R., Marrouche, N.F., 2012. Identification and acute targeting of gaps in atrial ablation lesion sets using a real-time magnetic resonance imaging system. *Circulation: Arrhythmia and Electrophysiology* 5, 1130–1135.
- Ravanelli, D., dal Piaz, E.C., Centonze, M., Casagrande, G., Marini, M., Del Greco, M., Karim, R., Rhode, K., Valentini, A., 2014. A novel skeleton based quantification and 3-D volumetric visualization of left atrium fibrosis using late gadolinium enhancement magnetic resonance imaging. *IEEE Transactions on Medical Imaging* 33, 566–576.
- Regazzoli, D., Ancona, F., Trevisi, N., Guarracini, F., Radinovic, A., Oppizzi, M., Marzi, A., Sora, N.C., Della Bella, P., Mazzone, P., et al., 2015. Left atrial appendage: physiology, pathology, and role as a therapeutic target. *BioMed Research International* 2015.
- Rhode, K., Karim, R., 2012. ISBI 2012: Left atrium fibrosis and scar segmentation challenge. <http://www.cardiacatlas.org/challenges/left-atrium-fibrosis-and-scar-segmentation-challenge/>.
- Rolf, S., Hindricks, G., Sommer, P., Richter, S., Arya, A., Bollmann, A., Kosiuk, J., Koutalas, E., 2014. Electroanatomical mapping of atrial fibrillation: Review of the current techniques and advances. *Journal of Atrial Fibrillation* 7.
- Saad, E.B., Cole, C.R., Marrouche, N.F., Dresing, T.J., PEREZ-LUGONES, A., Saliba, W.I., Schweikert, R.A., Klein, A., Rodriguez, L., Grimm, R., et al., 2002. Use of intracardiac echocardiography for prediction of chronic pulmonary vein stenosis after ablation of atrial fibrillation. *Journal of Cardiovascular Electrophysiology* 13, 986–989.
- Savioli, N., Montana, G., Lamata, P., 2018. V-fcn: volumetric fully convolution neural network for automatic atrial segmentation, in: *International Workshop on Statistical Atlases and Computational Models of the Heart*, Springer. pp. 273–281.
- Sibley, C.T., Noureldin, R.A., Gai, N., Nacif, M.S., Liu, S., Turkbey, E.B., Mudd, J.O., Van Der Geest, R.J., Lima, J.A., Halushka, M.K., et al., 2012. T1 mapping in cardiomyopathy at cardiac MR: comparison with endomyocardial biopsy. *Radiology* 265, 724–732.
- Siebertmair, J., Kholmovski, E.G., Marrouche, N., 2017. Assessment of left atrial fibrosis by late gadolinium enhancement magnetic resonance imaging: methodology and clinical implications. *JACC: Clinical Electrophysiology* 3, 791–802.
- Spragg, D.D., Khurram, I., Zimmerman, S.L., Yarmohammadi, H., Barcelon, B., Needleman, M., Edwards, D., Marine, J.E., Calkins, H., Nazarian, S., 2012. Initial experience with magnetic resonance imaging of atrial scar and co-registration with electroanatomic voltage mapping during atrial fibrillation: success and limitations. *Heart Rhythm* 9, 2003–2009.
- Suenari, K., Nakano, Y., Hirai, Y., Ogi, H., Oda, N., Makita, Y., Ueda, S., Kajihara, K., Tokuyama, T., Motoda, C., et al., 2013. Left atrial thickness under the catheter ablation lines in patients with paroxysmal atrial fibrillation: insights from 64-slice multidetector computed tomography. *Heart and Vessels* 28, 360–368.
- Taclas, J.E., Nezafat, R., Wylie, J.V., Josephson, M.E., Hsing, J., Manning, W.J., Peters, D.C., 2010. Relationship between intended sites of rf ablation and post-procedural scar in AF patients, using late gadolinium enhancement cardiovascular magnetic resonance. *Heart Rhythm* 7, 489–496.
- Taha, A.A., Hanbury, A., 2015. Metrics for evaluating 3D medical image segmentation: analysis, selection, and tool. *BMC Medical Imaging* 15, 29.
- Tao, Q., Ipek, E.G., Shahzad, R., Berendsen, F.F., Nazarian, S., van der Geest, R.J., 2016a. Fully automatic segmentation of left atrium and pulmonary veins in late gadolinium-enhanced MRI: Towards objective atrial scar assessment. *Journal of Magnetic Resonance Imaging* 44, 346–354.
- Tao, Q., Shahzad, R., Berendsen, F.F., van der Geest, R.J., 2016b. Automatic left atrial wall segmentation from contrast-enhanced CT angiography images, in: *International Workshop on Statistical Atlases and Computational Models of the Heart*, Springer. pp. 220–227.
- Tobon-Gomez, C., Geers, A.J., Peters, J., Weese, J., Pinto, K., Karim, R., Ammar, M., Daoudi, A., Margeta, J., Sandoval, Z., et al., 2015. Benchmark for algorithms segmenting the left atrium from 3D CT and MRI datasets. *IEEE Transactions on Medical Imaging* 34, 1460–1473.
- Toffanin, G., Scarabeo, V., Verlato, R., De Conti, F., Zampiero, A.A., Piovesana, P., 2006. Transoesophageal echocardiographic evaluation of pulmonary vein anatomy in patients undergoing ostial radiofrequency catheter ablation for atrial fibrillation: a comparison with magnetic resonance angiography. *Journal of Cardiovascular Medicine* 7, 748–752.
- Tops, L.F., Schalij, M.J., Bax, J.J., 2010. Imaging and atrial fibrillation: the role of multimodality imaging in patient evaluation and management of atrial fibrillation. *European Heart Journal* 31, 542–551.
- Tsao, H., Wu, M., Huang, B., Lee, S., Lee, K., Tai, C., Lin, Y., Hsieh, M., Kuo, J., Lei, M., et al., 2005. Morphologic remodeling of pulmonary veins and left atrium after catheter ablation of atrial fibrillation: Insight from long-term follow-up of three-dimensional magnetic resonance imaging. *Journal of Cardiovascular Electrophysiology* 16, 7–12.
- Utah, 2012. Cardiac MRI data from the comprehensive arrhythmia research and management (CARMA) center at the University of Utah. <http://insight-journal.org/midas/%20collection/view/197/>.
- Veni, G., Elhabian, S.Y., Whitaker, R.T., 2017. Shapecut: Bayesian surface estimation using shape-driven graph. *Medical Image Analysis* 40, 11–29.
- de Vente, C., Veta, M., Razeghi, O., Niederer, S., Pluim, J., Rhode, K., Karim, R., 2018. Convolutional neural networks for segmentation of the left atrium from gadolinium-enhancement MRI images, in: *International Workshop on Statistical Atlases and Computational Models of the Heart*, Springer. pp. 348–356.
- Verma, A., Kilicaslan, F., Pisano, E., Marrouche, N.F., Fanelli, R., Brachmann, J., Geunther, J., Potenza, D., Martin, D.O., Cummings, J., et al., 2005a. Response of atrial fibrillation to pulmonary vein antrum isolation is directly related to resumption and delay of pulmonary vein conduction. *Circulation* 112, 627–635.
- Verma, A., Wazni, O.M., Marrouche, N.F., Martin, D.O., Kilicaslan, F., Minor, S., Schweikert, R.A., Saliba, W., Cummings, J., Burkhardt, J.D., et al., 2005b. Pre-existent left atrial scarring in patients undergoing pulmonary vein antrum isolation: an independent predictor of procedural failure. *Journal of the American College of Cardiology* 45, 285–292.
- Vesal, S., Ravikumar, N., Maier, A., 2018. Dilated convolutions in neural networks for left atrial segmentation in 3D gadolinium enhanced-MRI, in: *International Workshop on Statistical Atlases and Computational Models of the Heart*, Springer. pp. 319–328.
- Vinnakota, K.C., Bassingthwaite, J.B., 2004. Myocardial density and composition: a basis for calculating intracellular metabolite concentrations. *American Journal of Physiology-Heart and Circulatory Physiology* 286, H1742–H1749.
- Wang, C., Rajchl, M., Chan, A.D., Ukwatta, E., 2019a. An ensemble of U-net architecture variants for left atrial segmentation, in: *Medical Imaging 2019: Computer-Aided Diagnosis*, International Society for Optics and Photonics. p. 109500M.
- Wang, Y., Xiong, Z., Nalar, A., Hansen, B.J., Kharche, S., Seemann, G., Loewe, A., Fedorov, V.V., Zhao, J., 2019b. A robust computational framework for estimating 3D bi-atrial chamber wall thickness. *Computers in Biology and Medicine* 114, 103444.
- Whitaker, J., Rajani, R., Chubb, H., Gabrawi, M., Varela, M., Wright, M., Niederer, S., O'Neill, M.D., 2016. The role of myocardial wall thickness in atrial arrhythmogenesis. *Ep Europace* 18, 1758–1772.
- Wu, F., Li, L., Yang, G., Wong, T., Mohiaddin, R., Firmin, D., Keegan, J., Xu, L., Zhuang, X., 2018. Atrial fibrosis quantification based on maximum likelihood estimator of multivariate images, in: *International Conference on Medical Image Computing and Computer-Assisted Intervention*, Springer. pp. 604–612.
- Xia, Q., Yao, Y., Hu, Z., Hao, A., 2018. Automatic 3D atrial segmentation from

- GE-MRIs using volumetric fully convolutional networks, in: International Workshop on Statistical Atlases and Computational Models of the Heart, Springer. pp. 211–220.
- Xiong, Z., Fedorov, V.V., Fu, X., Cheng, E., Macleod, R., Zhao, J., 2018. Fully automatic left atrium segmentation from late gadolinium enhanced magnetic resonance imaging using a dual fully convolutional neural network. *IEEE Transactions on Medical Imaging* 38, 515–524.
- Xiong, Z., Xia, Q., Hu, Z., Huang, N., Bian, C., Zheng, Y., Vesal, S., Ravikumar, N., Maier, A., Yang, X., et al., 2020. A global benchmark of algorithms for segmenting the left atrium from late gadolinium-enhanced cardiac magnetic resonance imaging. *Medical Image Analysis*, 101832.
- Yamada, T., Murakami, Y., Okada, T., Okamoto, M., Shimizu, T., Toyama, J., Yoshida, Y., Tsuboi, N., Ito, T., Muto, M., et al., 2006. Incidence, location, and cause of recovery of electrical connections between the pulmonary veins and the left atrium after pulmonary vein isolation. *Europace* 8, 182–188.
- Yang, G., Chen, J., Gao, Z., Li, S., Ni, H., Angelini, E., Wong, T., Mohiaddin, R., Nyktari, E., Wage, R., et al., 2020. Simultaneous left atrium anatomy and scar segmentations via deep learning in multiview information with attention. *Future Generation Computer Systems* 107, 215–228.
- Yang, G., Zhuang, X., Khan, H., Haldar, S., Nyktari, E., Li, L., Wage, R., Ye, X., Slabaugh, G., Mohiaddin, R., et al., 2018a. Fully automatic segmentation and objective assessment of atrial scars for long-standing persistent atrial fibrillation patients using late gadolinium-enhanced MRI. *Medical Physics* 45, 1562–1576.
- Yang, G., Zhuang, X., Khan, H., Haldar, S., Nyktari, E., Li, L., Ye, X., Slabaugh, G., Wong, T., Mohiaddin, R., et al., 2017a. Differentiation of pre-ablation and post-ablation late gadolinium-enhanced cardiac MRI scans of longstanding persistent atrial fibrillation patients, in: *Medical Imaging 2017: Computer-Aided Diagnosis*, International Society for Optics and Photonics. p. 1013400.
- Yang, G., Zhuang, X., Khan, H., Haldar, S., Nyktari, E., Ye, X., Slabaugh, G., Wong, T., Mohiaddin, R., Keegan, J., et al., 2017b. A fully automatic deep learning method for atrial scarring segmentation from late gadolinium-enhanced MRI images, in: *2017 IEEE 14th International Symposium on Biomedical Imaging (ISBI 2017)*, IEEE. pp. 844–848.
- Yang, X., Wang, N., Wang, Y., Wang, X., Nezafat, R., Ni, D., Heng, P.A., 2018b. Combating uncertainty with novel losses for automatic left atrium segmentation, in: *International Workshop on Statistical Atlases and Computational Models of the Heart*, Springer. pp. 246–254.
- Yu, L., Wang, S., Li, X., Fu, C.W., Heng, P.A., 2019. Uncertainty-aware self-ensembling model for semi-supervised 3D left atrium segmentation, in: *International Conference on Medical Image Computing and Computer-Assisted Intervention*, Springer. pp. 605–613.
- Zhang, Q., Wang, J.f., Dong, Q.q., Yan, Q., Luo, X.h., Wu, X.y., Liu, J., Sun, Y.p., 2017. Evaluation of left atrial volume and function using single-beat real-time three-dimensional echocardiography in atrial fibrillation patients. *BMC Medical Imaging* 17, 44.
- Zhao, J., Hansen, B.J., Wang, Y., Csepe, T.A., Sul, L.V., Tang, A., Yuan, Y., Li, N., Bratasz, A., Powell, K.A., et al., 2017. Three-dimensional integrated functional, structural, and computational mapping to define the structural “fingerprints” of heart-specific atrial fibrillation drivers in human heart *ex vivo*. *Journal of the American Heart Association* 6, e005922.
- Zhao, J., Xiong, Z., 2018. MICCAI 2018: Atrial segmentation challenge. <http://atriaseg2018.cardiacatlas.org/>.
- Zhu, L., Gao, Y., Yezzi, A., Tannenbaum, A., 2013. Automatic segmentation of the left atrium from mr images via variational region growing with a moments-based shape prior. *IEEE Transactions on Image Processing* 22, 5111–5122.
- Zhuang, X., 2019. Multivariate mixture model for myocardial segmentation combining multi-source images. *IEEE Transactions on Pattern Analysis and Machine Intelligence* 41, 2933–2946.
- Zhuang, X., Li, L., Payer, C., Štern, D., Urschler, M., Heinrich, M.P., Oster, J., Wang, C., Smedby, Ö., Bian, C., et al., 2019. Evaluation of algorithms for multi-modality whole heart segmentation: an open-access grand challenge. *Medical Image Analysis* 58, 101537.